Global indicator data tracking changes in species-level biodiversity persistence, ecosystem resilience under climate change, and protected-area representativeness and connectedness

Running title: Global biodiversity indicator data

Chris Ware[1]*, Roozbeh Valavi[2], Mathew Vickers[3], Katherine, M. Giljohann[2], Karel Mokany[3], Andy Purvis[4], Patrick Walkden[4], Adriana De Palma[4], Connor Duffin[4], Sara Contu[4], Tom Harwood[5], Andrew Hoskins[6,7,8], Simon Ferrier[3]

1. CSIRO, Sandy Bay, TAS 7005, Australia
2. CSIRO, Clayton, VIC 3168, Australia
3. CSIRO, PO Box 1700, Canberra, ACT, 2601, Australia
4. Biodiversity Futures Lab, Natural History Museum, London, SW7 5BD, UK
5. Environmental Change Institute, University of Oxford, OX1 3QY, UK
6. North Australian Indigenous Land and Sea Management Alliance Ltd (NAILSMA)
7. School of the Environment, University of Queensland
8. College of Public Health, Medical and Vet Sciences, James Cook University

* Corresponding author: chris.ware@csiro.au

Acknowledgements

This work was supported by funding from the Science and Industry Endowment Fund (SIEF).

Abstract

Motivation

Biodiversity indicator data that are transparent, meaningful and up to date are important for tracking progress in achieving biodiversity targets and goals under the Kunming-Montreal Global Biodiversity Framework, and for identifying the degree to which further action is required.

Main types of variable contained

Output and summary data are provided for four biodiversity indicators: (i) the Biodiversity Habitat Index (BHI); (ii) the Bioclimatic Ecosystem Resilience Index (BERI); (iii) the Protected Area Representativeness and Connectedness Index for representativeness (PARC-representativeness); and (iv) the Protected Area Representativeness and Connectedness Index for connectedness (PARC-connectedness). The ecosystem condition data used in calculating these indicators are also provided.

Spatial location and grain

All global terrestrial areas excluding Antarctica, at ≈1 km (30 arcsecond) spatial resolution. Indicator values are also summarised and provided for all countries of the world, and for each of the biomes occurring within these countries.

Time period and grain

Annual from 2000 to 2024.

Major taxa and level of measurement

The indicators are calculated using community-level models of compositional dissimilarity based on data for > 400,000 species of terrestrial vascular plants, vertebrates and invertebrates.

Software format

Code is provided in Python and R to enable appropriate derivation of indicator values for any region of interest, such as a country or an ecosystem type.

Keywords

Biodiversity, indicators, Kunming-Montreal Global Biodiversity Framework, terrestrial, global, ecosystem condition, extinction, ecosystem resilience, climate change, protected areas.

Background

In responding to the current biodiversity crisis (Díaz et al. 2019; IPBES 2019; Leclère et al. 2020), goals and targets to halt and reverse declines in biodiversity have been established, most notably through the Kunming-Montreal Global Biodiversity Framework (KM-GBF) (CBD 2022b). Rigorous, meaningful and up-to-date biodiversity indicators are important for tracking progress on achieving biodiversity targets and for identifying the degree to which further action is required. The monitoring framework for the KM-GBF (CBD 2022a) established headline, component and complementary indicators relevant for quantifying changes in biodiversity status and management as relevant to each goal and target. Many of these indicators are still in development, and not all of the rest yet have global time series data (UNEP-WCMC 2025) .

Here we provide updated data generated for four indicators presently included as component indicators in the KM-GBF monitoring framework (Goal A, Targets 2,3, and 8, (CBD 2022a)): (i) the Biodiversity Habitat Index (BHI) (ii) the Bioclimatic Ecosystem Resilience Index (BERI); (iii) the Protected Area Representativeness and Connectedness Index for representativeness (PARC-representativeness), and; (iv) the Protected Area Representativeness and Connectedness Index for connectedness (PARC-connectedness). These indicators provide a system-level view of change in biodiversity protection, expected persistence, and resilience in the face of climate change. A key strength of the indicators lies in the way they integrate assessment of changes in multiple components of the KM-GBF goals (Ferrier 2025). For example, both the BHI and BERI integrate assessment of how species-level biodiversity is expected to be affected by changes in the area, integrity, and connectivity of ecosystems, each of which are to be maintained, enhanced, or restored under Goal A (CBD 2022a; Ferrier 2025). For all four of these indicators, we provide data annually (2000-2024) for all terrestrial areas (excluding the Antarctic) at 30 arcsecond spatial resolution (≈1 km at the equator).

Methods

Overview

The four biodiversity indicators are derived from the following key input datasets, in different combinations (see Figure S1.1 in Supporting Information):

- Spatial layers representing predictions from a generalized dissimilarity model (GDM) of the difference in species composition expected between ecological communities at any two locations (30 arcsecond grid-cells) on the planet under current climatic conditions
- Spatial layers representing predictions from a GDM of differences in species composition expected under alternative future climate scenarios
- A spatial layer representing ecosystem condition for each location (one layer for each year of interest), estimated from land-use
- A spatial layer representing the estimated connectivity-adjusted ecosystem condition for each location (one layer for each year)
- Spatial data representing the coverage of protected areas (one layer for each year).

The methods and data presented here relate to the generation of the four biodiversity indicators for all terrestrial areas globally (excluding the Antarctic) at ≈1 km (30 arcsecond) spatial resolution at an annual timestep for the period 2000-2024. These global data can be used to derive summary indicator values for any user-defined spatial reporting area.

The methods applied here build on, and refine, those described in previous data publications and applications of these indicators (Di Marco, Ferrier, et al. 2019; Di Marco, Harwood, et al. 2019; Ferrier et al. 2020; Harwood et al. 2022; Hoskins et al. 2020). These refinements relate particularly to improving the

computational simplicity and efficiency of the global implementation of the indicator calculations by: (i) employing a single GDM across all taxa in each biogeographic realm; and (ii) summarising the continuous GDM spatial predictions using a discrete classification. The methods are presented in detail in Appendix S1, with a summary provided below.

Data inputs – biodiversity models

Previously developed GDMs (Hoskins et al. 2020) derived from data for > 400,000 species of terrestrial vertebrates, invertebrates and vascular plants globally were synthesised into a single all-taxa GDM for each of seven terrestrial biogeographic realms (Olson et al. 2001) (Appendix S1, Table S1.2-3). These steps were undertaken to reduce computational complexity and to more readily enable reporting of indicators representing a wider cross-section of biodiversity. The synthesised GDMs were used to generate spatial prediction layers for both 'current' climate (1960–1990 period) (Hijmans et al. 2005) and six climate scenarios centred on 2050 (as per Ferrier et al. (2020)). Each set of GDM spatial prediction layers were then classified using k-means (Ikotun et al. 2023) to produce sets of grid cells of very high predicted pairwise compositional similarity, with these classes used to enhance the computational efficiency of some of the indicator calculations (see below).

Data inputs – ecosystem condition

Global spatial layers of ecosystem condition for each year (2000–2024) were derived by first estimating the proportional coverage of 12 land-use classes in each ≈1 km grid cell modelled as a function of dynamic predictors derived from remote sensing (Di Marco, Harwood, et al. 2019; Hoskins et al. 2016), using statistical downscaling models trained with data from the Land-Use Harmonization project (Hurtt et al. 2020). Algorithmic adjustments were then applied to align cropping and urban proportions with the European Space Agency's Climate Change Initiative land cover data (ESA 2017) and also to prevent unrealistic increases in primary vegetation (Appendix S1). These land-use proportions were converted to an estimate of ecosystem condition for each grid cell in a given year using coefficients from a model fitted specifically for this purpose to data from the PREDICTS project's meta-analysis of local land-use impacts on biodiversity (Hudson et al. 2017; Newbold et al. 2016), in which land-use class was the anthropogenic factor considered. Each land-use coefficient estimates the proportion (0 to 1) of native species originally occurring at a location which are expected to remain given the current land-use of that location – capped at a maximum of 1 for primary vegetation (Table S1.4).

To derive the BHI indicator, the ecosystem condition spatial layer for each year is further adjusted to account for the effects of connectivity to surrounding areas of habitat for each pixel. This connectivity-adjusted ecosystem condition layer is created using an extension of the cost-benefit approach (CBA) developed by (Drielsma, Ferrier, and Manion 2007) which is based on principles of meta-population ecology. Multi-resolution graph-based analysis was used to enhance the computational efficiency of this extended connectivity analysis (Appendix S1, Figure S1.2).

Data inputs – protected areas and intact natural ecosystems data

Both PARC indices (PARC-representativeness and PARC-connectedness) rely on spatial data identifying where terrestrial protected areas and "Other Area-Based Conservation Measures" (OECMs) are located globally. The World Database on Protected Areas (WDPA, https://www.protectedplanet.net/en) and World Database on Other Area-Based Conservation Measures (WD-OECM, https://www.protectedplanet.net/en) were used as the bases for this, with annual (2000-2024) global layers prepared which aligned with our ≈1 km grid (see Supporting Information). PARC-connectedness additionally requires spatial data identifying where intact natural ecosystems occur outside of protected areas and OECMs. For this, we used the estimates of ecosystem condition described above and assigned each grid cell the maximum of: 1) the proportion of that cell under protection; and 2) the cell's ecosystem condition.

Indicator calculation – the Biodiversity Habitat Index (BHI)

The BHI (UNEP-WCMC 2023b) estimates the level of species diversity expected to be retained within any given spatial reporting unit (e.g. a country, an ecosystem type, or the entire planet) as a function of the area, condition and connectivity of natural ecosystems across that unit (Allnutt et al. 2008; Di Marco, Harwood, et al. 2019; Ferrier et al. 2024; Mokany, Harwood, and Ferrier 2019). Results for the indicator are expressed as the proportion of species expected to persist (i.e. avoid extinction) over the long term, estimated using an extended form of species-area analysis which accounts for the predicted compositional similarity between grid cells and for connectivity-adjusted ecosystem condition (Appendix S1). The overall (summarised) BHI value for a given reporting unit (e.g. a country) is derived as a weighted geometric mean of cell-level scores within that region, with the weight of each grid cell reflecting the predicted compositional uniqueness of that cell. A global value can be calculated in the same way by considering all grid cells. For regions with known species richness, the BHI estimates can also be expressed as the number of species expected to persist over the long term by simply multiplying this estimated proportion by the total number of species known to occur in the region of interest. We demonstrate this for the globe by reporting both proportions and numbers of species expected to persist, using the value of 6.5 million terrestrial species globally, as calculated by Mora et al. (2011). Given the standard BHI calculation considers the contribution of grid cells outside the reporting region, we also derived a 'closed-system' BHI value for each country of the world, which will be influenced only by changes in connectivity-adjusted ecosystem condition for grid cells within that country.

Indicator calculation – the Bioclimatic Ecosystem Resilience Index (BERI)

The BERI (UNEP-WCMC 2023a) estimates the capacity of landscapes to retain species diversity in the face of climate change, as a function of the area, condition and connectivity of natural ecosystems across those landscapes (Ferrier et al. 2020; Harwood et al. 2022). The indicator assesses the extent to which any given spatial configuration of natural habitat will promote or hinder climate-induced shifts in biological distributions. It does this by analysing the functional connectivity of each grid-cell of natural habitat to areas of habitat in the surrounding landscape which are projected to support a similar assemblage of species under climate change to that currently associated with the cell of interest (Appendix S1). As with the BHI, regional BERI values are derived as weighted geometric means of cell-level scores within that region, and an additional 'closed-system' BERI value for each country is calculated using only the grid cells within that country.

Indicator calculation – PARC-representativeness

The PARC-representativeness index (UNEP-WCMC 2023c) assesses the extent to which a system of terrestrial protected areas and OECMs is ecologically representative of the full range of environmental and biological diversity present within any given spatial reporting unit (e.g. a country). For each grid cell, PARC-representativeness estimates the proportion of all ecologically-similar grid cells that are included in the protected-area system (Appendix S1). As with the BHI and BERI, regional PARC-representativeness values are derived as weighted geometric means of cell-level scores within that region, and an additional 'closed-system' PARC-representativeness value for each country is calculated based on data only for the grid cells within that country.

Indicator calculation – PARC-connectedness

The PARC-connectedness index (UNEP-WCMC 2023c) provides a measure of the extent to which protected areas and OECMs are functionally connected to one another and to other areas of intact natural ecosystems, thereby enhancing integration into the wider landscape. The PARC-connectedness score assigned to each protected cell is expressed as a proportion (0 to 1) of the maximum possible level of connectedness obtainable if that cell were surrounded by a continuous expanse of protection, and/or intact natural vegetation in the surrounding landscape (Appendix S1). PARC-connectedness for each grid

cell is calculated using the same cost-benefit approach as applied to derive connectivity-adjusted ecosystem condition (described above). Regional PARC-connectedness values are derived as the sum of cell-level scores for all cells falling within protected areas within that region divided by the number of cells within the region (Appendix S1). An additional 'closed-system' PARC- connectedness value for each country is calculated using only the grid cells within that country.

Data Access

Global gridded (GeoTIFF) datasets and summary (CSV) datasets for both countries and biomes nested with countries are available for non-commercial use via: https://doi.org/10.25919/fdn7-8n93 (Ware et al. 2025). Metadata is contained in Table S2. Summary indicator data and maps can also be viewed at https://shiny.csiro.au/BILBI-indicators/

Summary of the indicator data

Mapping of the gridded indicator data for the most recent year (2024) shows spatial patterns in expected biodiversity persistence (BHI; Fig. 1a), bioclimatic ecosystem resilience under climate change (BERI; Fig1b), representativeness of protected areas (PARC-representativeness; Fig. 1c), and connectedness of protected areas to other protected areas and to intact natural habitat across the broader landscape (PARC-connectedness; Fig. 1d). The highest values for BHI and BERI are in large regions of intact habitat, including the western Amazon and boreal ecosystems, while the lowest values are in regions with high intensity of human land-use, such as Europe, eastern North America and East Asia (Fig. 1a,b). Spatial patterns for PARC-representativeness and PARC connectedness broadly align with the spatial distribution of protected areas, though with important finer resolution variation (Fig. 1c,d).

Change in the indicator values over time, summarised for individual countries and globally, show decreases in BHI and BERI, associated with widespread increases in land-use intensity and reductions in ecosystem condition (Fig. 2a-c, Appendix S3). The BHI values indicate that 26 % of all terrestrial species globally (1.78 million species) are expected to eventually become extinct due to all past land use changes – an estimate which falls in between the one million species estimated to be threatened with extinction by the IPBES 2019 Global Assessment Report (IPBES 2019) and a more recent estimate of two million species (Hochkirch et al. 2023). Since 2000, the proportion of all terrestrial species expected to persist as estimated by the BHI has decreased by 1 % or 65,000 species (Appendix S3). Increases in the area of land under protection are responsible for increases in PARC-representativeness and PARC-connectedness over time (Fig. 2d,e).

Indicator data usage

All four indicators, along with the ecosystem condition data employed in deriving them, can be used by national or sub-national jurisdictions for reporting change in biodiversity within the context of the KM-GBF. The indicators, and ongoing yearly updates to them, can also be summarised for any set of ecosystem classes within any jurisdiction using the guidance code provided in Appendix S2 and S4 respectively. To demonstrate this, we provide summaries using the intersection of WWF biomes (Olson et al. 2001) and country borders (GADM, http://gadm.org/country) demonstrating this, but summaries could equally be derived using other ecosystem classification frameworks as they are developed (e.g. the Functional Ecosystem Groups from the Global Ecosystem Typology (Keith et al. 2022) and/or are adopted in reporting frameworks under the KM-GBF.

Given the relatively fine spatial resolution of the gridded indicator data, and complete coverage of the terrestrial earth surface (with the exception of the Antarctic), the data are also potentially applicable to

ecosystem accounting aligned with the System of Environmental-Economic Accounting (Mokany et al. 2022, 2024; United Nations 2024), and various forms of corporate reporting (Mokany et al. 2025). Care is required in such applications, particularly when summarising the gridded indicators for multiple regions. Because biodiversity scales in an inherently non-additive manner, summary results for different regions (e.g. countries or ecosystem types) cannot be derived by simply averaging indicator values across grid cells falling within each region of interest region. Guidance on the required calculations are outlined in Appendix S2, and example code provided in https://doi.org/10.25919/fdn7-8n93. Combining results for multiple locations with different baseline years, such as may be required for corporate reporting use-cases, must also consider this need to accommodate the non-additive nature of regionally summarised indictors (Mokany et al. 2025). For use in ecosystem accounting, it must be acknowledged that changes external to a region of interest will have bearing on the indicator results for that region. Finally, we note that while we consider the gridded data to be relatively fine spatial resolution for the purposes of biodiversity monitoring and assessment, the ≈1 km grid cells do not always represent coastlines or small islands well. Summaries focussed on these areas should be treated more cautiously.

The gridded indicator data for PARC-representativeness not only enable reporting but can also directly inform prioritisation of new protected areas. Expanding protected-area coverage across grid cells with the lowest PARC-representativeness values would be most effective in enhancing ecological representativeness under KM-GBF Target 3. Mapping of priorities for action can also be undertaken for the other biodiversity indicators presented here, such as identifying areas where ecosystem restoration would most effectively and efficiently enhance BHI or BERI results, though this would require additional customised analyses.

Extensions of the data and methods described here allow for projections of the BHI and BERI to be made under scenarios of different high-level policies (e.g. Di Marco et al. (2019)) or specific actions (e.g. Mokany et al. (2025)). Such projections can be used to explore how different actions (e.g. removal, protection, or restoration of natural habitat) may affect outcomes for biodiversity, thereby serving as a valuable planning tool. This forward-looking functionality is made possible by modelling how ecosystem condition will respond to any proposed action or set of actions, and then rederiving the indicators from those condition projections. The same functionality can also be used to model changes in the BHI and BERI expected to result from sets of actions which have already been, or are being, implemented (rather than just being considered), but for which insufficient time has elapsed for any resulting impacts to be reflected in the monitoring of ecosystem condition. While applying the indicators in this forward-looking mode requires data and analytical routines additional to those described here, this potential represents a significant strength of the overall approach, by allowing the same indicators used to monitor progress towards achieving goals, as a function of observed changes in ecosystem condition, to also be used to guide planning and decision making, and to additionally monitor the expected contribution that implemented actions – e.g. under the KM-GBF targets – are making to the achievement of goals (Ferrier 2025).

Evaluation of the indicators would ideally be performed by comparing generated estimates to independent empirical observations; however, this is challenging given such evaluation will only be feasible in decades to come as data on the retention of biodiversity over time is collected (Ferrier et al. 2020). Nevertheless, analytical components used in our indicator derivation have undergone empirical evaluation and been demonstrated to perform well. The GDM approach used to estimate spatial biodiversity patterns from species occurrence data has performed well when tested against independent biological survey data and mapped vegetation types and bioregions (Elith et al. 2006; Ware et al. 2018); our method of estimating land-use, which underpins ecosystem condition, has been shown to reproduce independent observations of land-use classes (Hoskins et al. 2016); and GDM-based projections of temporal change in the distribution of plant biodiversity, as a function of climate change, have also performed well when evaluated against fossil pollen data, and climatic reconstructions, from the past 20,000 years (Blois et al. 2013). Furthermore, in a comparative analysis of a range of global biodiversity indicators, results for the

BHI exhibited a statistically significant, and moderately strong, correlation with those for the Red List Index of species extinction risk (Stevenson et al. 2024).

References

Allnutt, T. F., S. Ferrier, G. Manion, G. V. N. Powell, T. H. Ricketts, B. L. Fisher, and F. Rakotondrainibe. 2008. "A Method for Quantifying Biodiversity Loss and Its Application to a 50-Year Record of Deforestation across Madagascar." *Conservation Letters* 1(4):173–81. doi:10.1111/j.1755-263X.2008.00027.x.

Blois, Jessica L., Phoebe L. Zarnetske, Matthew C. Fitzpatrick, and Seth Finnegan. 2013. "Climate Change and the Past, Present, and Future of Biotic Interactions." *Science* 341(6145):499–504. doi:10.1126/science.1237184.

CBD. 2022a. "Monitoring framework for the Kunming-Montreal Global Biodiversity Framework." CBD/COP/15/L.25.

CBD. 2022b. "The Kunming-Montreal Global Biodiversity Framework." CBD/COP/15/L.26.

Di Marco, M., S. Ferrier, T. D. Harwood, A. J. Hoskins, and J. E. M. Watson. 2019. "Wilderness areas halve the extinction risk of terrestrial biodiversity." *Nature* 573:582–85. doi:10.1038/s41586-019-1567-7.

Di Marco, M., T. D. Harwood, A. J. Hoskins, C. Ware, S. L. L. Hill, and S. Ferrier. 2019. "Projecting Impacts of Global Climate and Land-Use Scenarios on Plant Biodiversity Using Compositional-Turnover Modelling." *Global Change Biology* 25(8):2763–78. doi:10.1111/gcb.14663.

Díaz, Sandra, Josef Settele, Eduardo S. Brondízio, Hien T. Ngo, John Agard, Almut Arneth, Patricia Balvanera, Kate A. Brauman, Stuart H. M. Butchart, Kai M. A. Chan, Lucas A. Garibaldi, Kazuhito Ichii, Jianguo Liu, Suneetha M. Subramanian, Guy F. Midgley, Patricia Miloslavich, Zsolt Molnár, David Obura, Alexander Pfaff, Stephen Polasky, Andy Purvis, Jona Razzaque, Belinda Reyers, Rinku Roy Chowdhury, Yunne-Jai Shin, Ingrid Visseren-Hamakers, Katherine J. Willis, and Cynthia N. Zayas. 2019. "Pervasive Human-Driven Decline of Life on Earth Points to the Need for Transformative Change." *Science* 366(6471):eaax3100. doi:10.1126/science.aax3100.

Drielsma, Michael, Simon Ferrier, and Glenn Manion. 2007. "A Raster-Based Technique for Analysing Habitat Configuration: The Cost–Benefit Approach." *Ecological Modelling* 202(3–4):324–32. doi:10.1016/j.ecolmodel.2006.10.016.

Elith, Jane, Catherine H. Graham, Robert P. Anderson, Miroslav Dudík, Simon Ferrier, Antoine Guisan, Robert J. Hijmans, Falk Huettmann, John R. Leathwick, Anthony Lehmann, Jin Li, Lucia G. Lohmann, Bette A. Loiselle, Glenn Manion, Craig Moritz, Miguel Nakamura, Yoshinori Nakazawa, Jacob McC. M. Overton, A. Townsend Peterson, Steven J. Phillips, Karen Richardson, Ricardo Scachetti-Pereira, Robert E. Schapire, Jorge Soberón, Stephen Williams, Mary S. Wisz, and Niklaus E. Zimmermann. 2006. "Novel Methods Improve Prediction of Species' Distributions from Occurrence Data." *Ecography* 29(2):129–51. doi:10.1111/j.2006.0906-7590.04596.x.

ESA. 2017. *ESA Land Cover CCI Product User Guide Version 2*. *Technical Report.* maps.elie.ucl.ac.be/CCI/viewer/download/ESACCI-LC-Ph2-PUGv2_2.0.pdf.

Ferrier, S., T. D. Harwood, C. Ware, and A. J. Hoskins. 2020. "A Globally Applicable Indicator of the Capacity of Terrestrial Ecosystems to Retain Biological Diversity under Climate Change: The Bioclimatic Ecosystem Resilience Index." *Ecological Indicators* 117:106554. doi:10.1016/j.ecolind.2020.106554.

Ferrier, S., C. Ware, J. M. Austin, H. S. Grantham, T. D. Harwood, and J. E. M. Watson. 2024. "Ecosystem Extent Is a Necessary but Not Sufficient Indicator of the State of Global Forest Biodiversity." *Conservation Letters* 17(5):13045. doi:10.1111/conl.13045.

Ferrier, Simon. 2025. "A Nature-positive World Is More than the Sum of Its Parts." *Methods in Ecology and Evolution* 2041-210x.70153. doi:10.1111/2041-210x.70153.

Harwood, T., J. Love, M. Drielsma, C. Brandon, and S. Ferrier. 2022. “Staying Connected: Assessing the Capacity of Landscapes to Retain Biodiversity in a Changing Climate.” *Landscape Ecology* 37(12):3123–39. doi:10.1007/s10980-022-01534-5.

Hijmans, Robert J., Susan E. Cameron, Juan L. Parra, Peter G. Jones, and Andy Jarvis. 2005. “Very High Resolution Interpolated Climate Surfaces for Global Land Areas.” *International Journal of Climatology* 25(15):1965–78. doi:10.1002/joc.1276.

Hochkirch, Axel, Melanie Bilz, Catarina C. Ferreira, Anja Danielczak, David Allen, Ana Nieto, Carlo Rondinini, Kate Harding, Craig Hilton-Taylor, Caroline M. Pollock, Mary Seddon, Jean-Christophe Vié, Keith N. A. Alexander, Emily Beech, Manuel Biscoito, Yoan Braud, Ian J. Burfield, Filippo Maria Buzzetti, Marta Cálix, Kent E. Carpenter, Ning Labbish Chao, Dragan Chobanov, Maarten J. M. Christenhusz, Bruce B. Collette, Mia T. Comeros-Raynal, Neil Cox, Matthew Craig, Annabelle Cuttelod, William R. T. Darwall, Benoit Dodelin, Nicholas K. Dulvy, Eve Englefield, Michael F. Fay, Nicholas Fettes, Jörg Freyhof, Silvia García, Mariana García Criado, Michael Harvey, Nick Hodgetts, Christina Ieronymidou, Vincent J. Kalkman, Shelagh P. Kell, James Kemp, Sonia Khela, Richard V. Lansdown, Julia M. Lawson, Danna J. Leaman, Joana Magos Brehm, Nigel Maxted, Rebecca M. Miller, Eike Neubert, Baudewijn Odé, David Pollard, Riley Pollom, Rob Pople, Juan José Presa Asensio, Gina M. Ralph, Hassan Rankou, Malin Rivers, Stuart P. M. Roberts, Barry Russell, Alexander Sennikov, Fabien Soldati, Anna Staneva, Emilie Stump, Andy Symes, Dmitry Telnov, Helen Temple, Andrew Terry, Anastasiya Timoshyna, Chris Van Swaay, Henry Väre, Rachel H. L. Walls, Luc Willemse, Brett Wilson, Jemma Window, Emma G. E. Wright, and Thomas Zuna-Kratky. 2023. “A Multi-Taxon Analysis of European Red Lists Reveals Major Threats to Biodiversity” edited by N. Dahanukar. *PLOS ONE* 18(11):e0293083. doi:10.1371/journal.pone.0293083.

Hoskins, A. J., A. Bush, J. Gilmore, T. Harwood, L. N. Hudson, C. Ware, and S. Ferrier. 2016. “Downscaling Land-Use Data to Provide Global 30’’ Estimates of Five Land-Use Classes.” *Ecology and Evolution* 6(9):3040–55. doi:10.1002/ece3.2104.

Hoskins, A. J., T. D. Harwood, C. Ware, K. J. Williams, J. J. Perry, N. Ota, and S. Ferrier. 2020. “BILBI: Supporting Global Biodiversity Assessment through High-Resolution Macroecological Modelling.” *Environmental Modelling & Software* 132:104806. doi:10.1016/j.envsoft.2020.104806.

Hudson, L. N., T. Newbold, S. Contu, S. L. L. Hill, I. Lysenko, A. Palma, and A. Purvis. 2017. “The Database of the PREDICTS (Projecting Responses of Ecological Diversity In Changing Terrestrial Systems) Project.” *Ecology and Evolution* 7(1):145–88. doi:10.1002/ece3.2579.

Hurtt, George C., Louise Chini, Ritvik Sahajpal, Steve Frolking, Benjamin L. Bodirsky, Katherine Calvin, Jonathan C. Doelman, Justin Fisk, Shinichiro Fujimori, Kees Klein Goldewijk, Tomoko Hasegawa, Peter Havlik, Andreas Heinimann, Florian Humpenöder, Johan Jungclaus, Jed O. Kaplan, Jennifer Kennedy, Tamás Krisztin, David Lawrence, Peter Lawrence, Lei Ma, Ole Mertz, Julia Pongratz, Alexander Popp, Benjamin Poulter, Keywan Riahi, Elena Shevliakova, Elke Stehfest, Peter Thornton, Francesco N. Tubiello, Detlef P. Van Vuuren, and Xin Zhang. 2020. “Harmonization of Global Land Use Change and Management for the Period 850–2100 (LUH2) for CMIP6.” *Geoscientific Model Development* 13(11):5425–64. doi:10.5194/gmd-13-5425-2020.

Ikotun, A. M., A. E. Ezugwu, L. Abualigah, B. Abuhaija, and J. Heming. 2023. “K-Means Clustering Algorithms: A Comprehensive Review, Variants Analysis, and Advances in the Era of Big Data.” *Information Sciences* 622:178–210. doi:10.1016/j.ins.2022.11.139.

IPBES. 2019. *Global Assessment Report on Biodiversity and Ecosystem Services of the Intergovernmental Science-Policy Platform on Biodiversity and Ecosystem Services*. edited by E. Brondizio, S. Diaz, J. Settele, and H. T. Ngo. Zenodo. doi:10.5281/ZENODO.3831673.

Keith, David A., José R. Ferrer-Paris, Emily Nicholson, Melanie J. Bishop, Beth A. Polidoro, Eva Ramirez-Llodra, Mark G. Tozer, Jeanne L. Nel, Ralph Mac Nally, Edward J. Gregr, Kate E. Watermeyer, Franz Essl, Don Faber-Langendoen, Janet Franklin, Caroline E. R. Lehmann, Andrés Etter, Dirk J. Roux, Jonathan S. Stark, Jessica A. Rowland, Neil A. Brummitt, Ulla C. Fernandez-Arcaya, Iain M. Suthers, Susan K. Wiser, Ian Donohue, Leland J. Jackson, R. Toby Pennington, Thomas M. Iliffe, Vasilis Gerovasileiou, Paul Giller, Belinda J. Robson, Nathalie Pettorelli, Angela Andrade, Arild Lindgaard, Teemu Tahvanainen, Aleks Terauds, Michael A. Chadwick, Nicholas J. Murray, Justin Moat, Patricio Pliscoff, Irene Zager, and Richard T. Kingsford. 2022. "A Function-Based Typology for Earth's Ecosystems." *Nature* 610(7932):513–18. doi:10.1038/s41586-022-05318-4.

Leclère, D., M. Obersteiner, M. Barrett, S. H. M. Butchart, A. Chaudhary, A. Palma, and L. Young. 2020. "Bending the Curve of Terrestrial Biodiversity Needs an Integrated Strategy." *Nature* 585(7826):551–56. doi:10.1038/s41586-020-2705-y.

Mokany, K., T. D. Harwood, and S. Ferrier. 2019. "Improving Links between Environmental Accounting and Scenario-Based Cumulative Impact Assessment for Better-Informed Biodiversity Decisions." *Journal of Applied Ecology* 56(12):2732–41. doi:10.1111/1365-2664.13506.

Mokany, K., C. Ware, T. D. Harwood, R. K. Schmidt, and S. Ferrier. 2022. "Habitat-Based Biodiversity Assessment for Ecosystem Accounting in the Murray–Darling Basin." *Conservation Biology* 36(5):13915. doi:10.1111/cobi.13915.

Mokany, K., C. Ware, R. Valavi, K. Giljohann, S. Ferrier, C. Stitzlein, and G. Mata. 2025. "A Habitat-Based Approach to Reporting the Direct Impacts of an Organization on Biodiversity." *Conservation Biology* 70071. doi:10.1111/cobi.70071.

Mokany, K., C. Ware, M. Vickers, K. M. Giljohann, Tetreault-Campbell S, A. Richards, and B. Schmidt. 2024. "Methods for Developing National Biodiversity Data for Ecosystem Accounting in Australia."

Mora, Camilo, Derek P. Tittensor, Sina Adl, Alastair G. B. Simpson, and Boris Worm. 2011. "How Many Species Are There on Earth and in the Ocean?" edited by G. M. Mace. *PLoS Biology* 9(8):e1001127. doi:10.1371/journal.pbio.1001127.

Newbold, T., L. N. Hudson, S. L. L. Hill, S. Contu, C. L. Gray, J. P. W. Scharlemann, and A. Purvis. 2016. "Global Patterns of Terrestrial Assemblage Turnover within and among Land Uses." *Ecography* 39(12):1151–63. doi:10.1111/ecog.01932.

Olson, D. M., E. Dinerstein, E. D. Wikramanayake, N. D. Burgess, G. V. N. Powell, E. C. Underwood, and K. R. Kassem. 2001. "Terrestrial Ecoregions of the World: A New Map of Life on Earth: A New Global Map of Terrestrial Ecoregions Provides an Innovative Tool for Conserving Biodiversity." *Bioscience* 51(11):933–38. doi:10.1641/0006-3568(2001)051.

Stevenson, Simone L., Kate Watermeyer, Simon Ferrier, Elizabeth A. Fulton, Hui Xiao, and Emily Nicholson. 2024. "Corroboration and Contradictions in Global Biodiversity Indicators." *Biological Conservation* 290:110451. doi:10.1016/j.biocon.2024.110451.

UNEP-WCMC. 2023a. "Indicators for the Kunming-Montreal Global Biodiversity Framework: Metadata Factsheet for the Bioclimatic Ecosystem Resilience Index." https://gbf-indicators.org/metadata/other/8-4-C

UNEP-WCMC. 2023b. "Indicators for the Kunming-Montreal Global Biodiversity Framework: Metadata Factsheet for the Biodiversity Habitat Index." https://gbf-indicators.org/metadata/other/A-4-C

UNEP-WCMC. 2023c. “Indicators for the Kunming-Montreal Global Biodiversity Framework: Metadata Factsheet for the Protected Area Representativeness and Connectedness (PARC) Indices.” https://gbf-indicators.org/metadata/other/A-5-C

UNEP-WCMC. 2025. “Indicators for the Kunming – Montreal Global Biodiversity Framework.” https://www.gbf-indicators.org/

United Nations. 2024. “System of Environmental-Economic Accounting—Ecosystem Accounting (SEEA EA). Statistical Papers.” *Series F* (124). https://seea.un.org/ecosystem-accounting.

Ware, C., Vickers, M., Valavi, R., Giljohann, K., Mokany, K., Purvis, A., Walkden, P., De Palma, A., Duffin, C., Contu, S., Harwood, T., Hoskins, A., and Ferrier, S. 2025. “Global Biodiversity Indicator Data for BHI, BERI, PARC-Representativeness, PARC-Connectedness and Ecosystem Condition (2000-2024). v1. CSIRO. Data Collection.” CSIRO Data Access Portal. https://doi.org/10.25919/fdn7-8n93.

Ware, Chris, Kristen J. Williams, Jo Harding, Brian Hawkins, Thomas Harwood, Glenn Manion, Genevieve C. Perkins, and Simon Ferrier. 2018. “Improving Biodiversity Surrogates for Conservation Assessment: A Test of Methods and the Value of Targeted Biological Surveys” edited by E. Di Minin. *Diversity and Distributions* 24(9):1333–46. doi:10.1111/ddi.12766.

Data and Code Availability Statement

The spatial layers providing indicator values for each grid cell in each year (2000-2024) are available for non-commercial use from CSIRO's Data Access Portal: https://doi.org/10.25919/fdn7-8n93 (Ware et al. 2025). Summary indicator values for each country are also provided in the supporting information (Appendix S3). Guidance on deriving regional summaries along with code are also available from CSIRO's Data Access Portal: https://doi.org/10.25919/fdn7-8n93 (Ware et al. 2025).

Figures

a) Biodiversity Habitat Index (BHI)

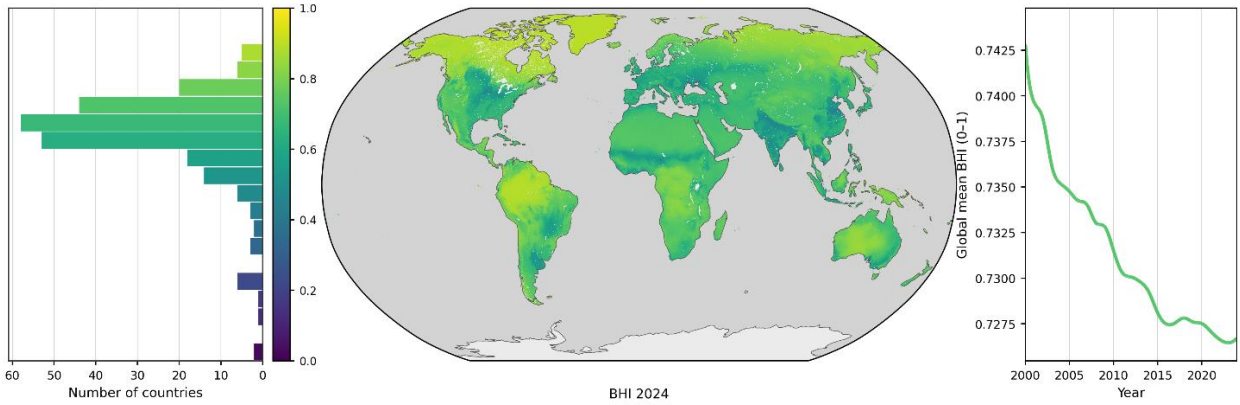

b) Bioclimatic Ecosystem Resilience Index (BERI)

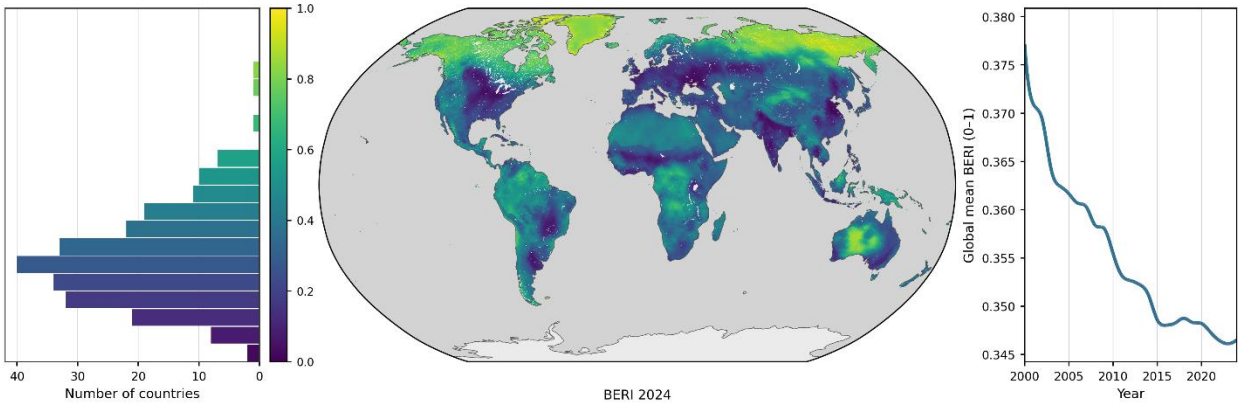

c) Protected Area Representativeness and Connectivity Index for representativeness (PARC-representativeness)

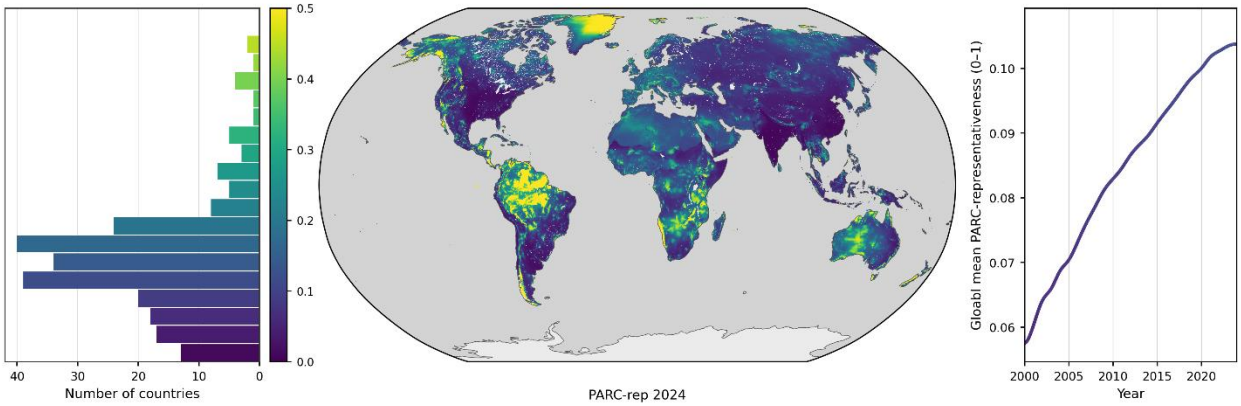

d) Protected Area Representativeness and Connectivity Index for connectedness (PARC-connectedness)

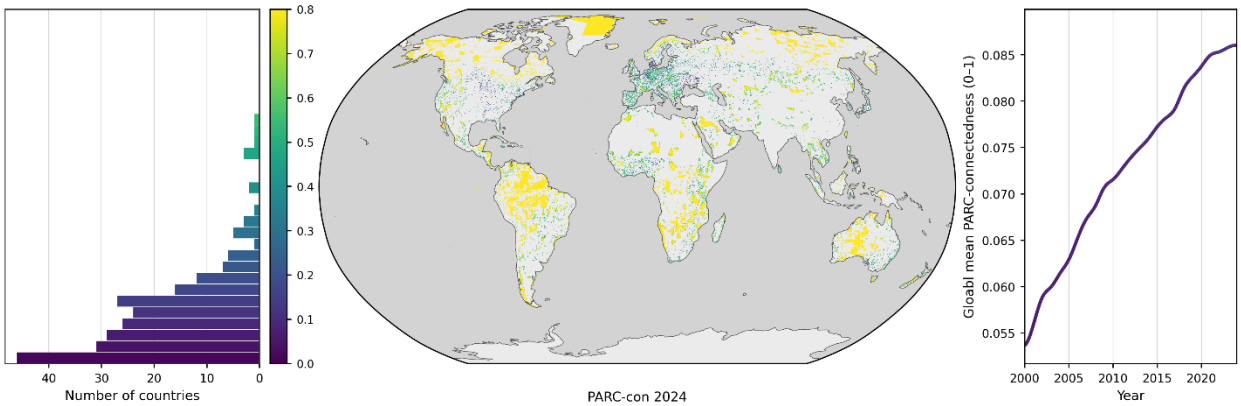

Figure 1. Country indicator distributions, gridded indicator data maps, and global annual trends for: **a)** the Biodiversity Habitat Index (BHI); **b).** the Bioclimatic Ecosystem Resilience Index (BERI); **c)** the Protected Area Representativeness and Connectedness Index for representativeness (PARC-representativeness); and **d)** the Protected Area Representativeness and Connectedness Index for connectedness (PARC-connectedness). For each indicator, the left panel depicts the distribution of indicator values summarised by country for the year 2024; the middle panel shows the mapped indicator values for the year 2024; and the right panel shows the annual global trend of mean indicator values from 2000-2024.

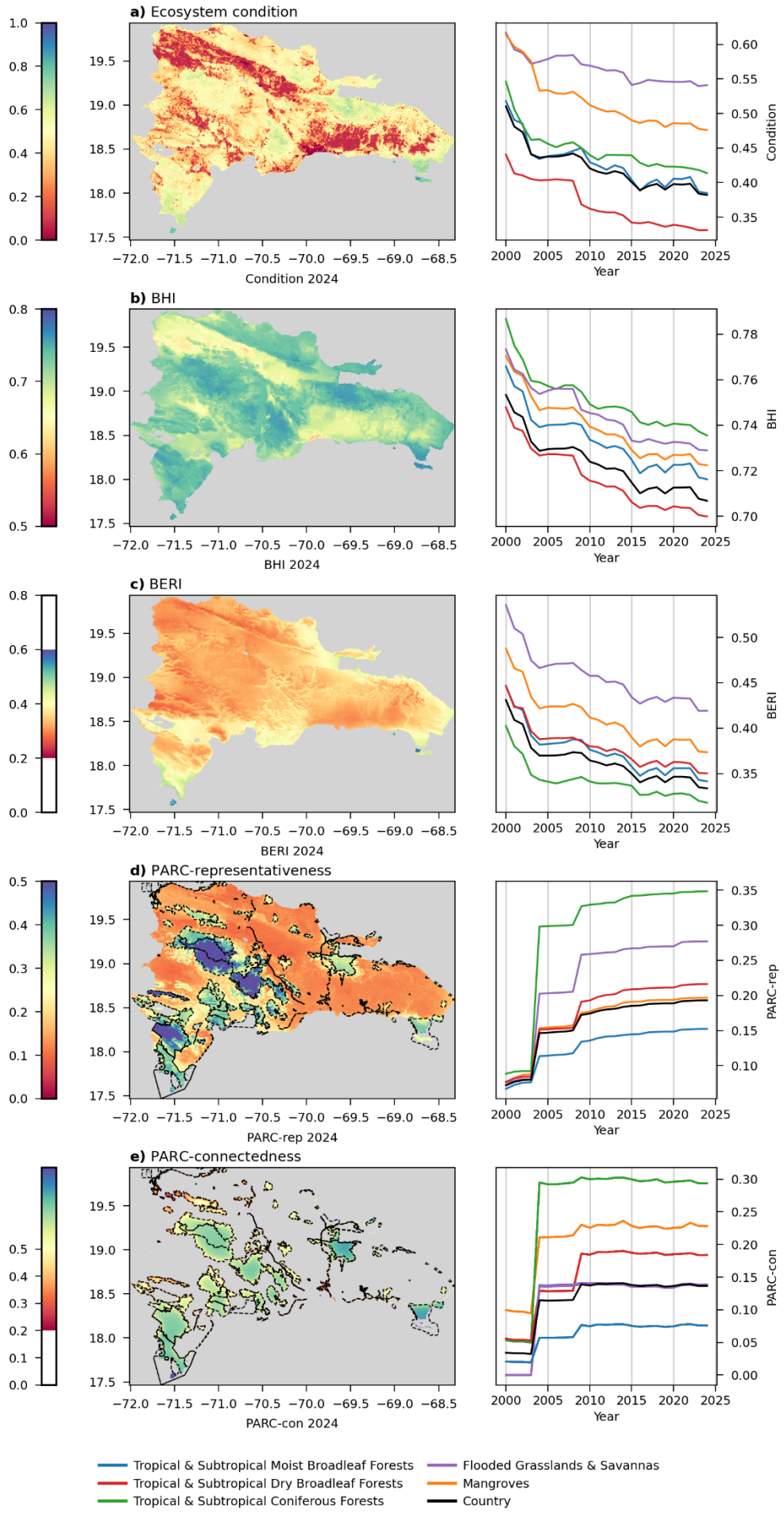
a) Ecosystem condition
Condition 2024
Condition
Year
b) BHI
BHI 2024
BHI
Year
c) BERI
BERI 2024
BERI
Year
d) PARC-representativeness
PARC-rep 2024
PARC-rep
Year
e) PARC-connectedness
PARC-con 2024
PARC-con
Year
Tropical & Subtropical Moist Broadleaf Forests
Tropical & Subtropical Dry Broadleaf Forests
Tropical & Subtropical Coniferous Forests
Flooded Grasslands & Savannas
Mangroves
Country

Figure 2. Example country-level maps revealing detail in the spatial patterns of indicators along with change charts summarised by biomes. Maps and chart values are shown for the Dominican Republic for: **a)** ecosystem condition; **b)** the Biodiversity Habitat Index (BHI); **c)** the Bioclimatic Ecosystem Resilience Index (BERI); **d)** the Protected Area Representativeness and Connectedness Index for representativeness (PARC-representativeness); and **e)** the Protected Area Representativeness and Connectedness Index for connectedness (PARC-connectedness). Lines in the line charts represent the different biomes found in the Dominican Republic (see bottom of figure for biome names). Habitat loss and fragmentation are more pronounced in the flatter more densely populated regions of the Dominican Republic (shown in more yellow-to-red colours in panel a), whereas the more mountainous regions retain greater levels of intact habitat. Panel b) demonstrates how, when spatial patterns of habitat condition are combined with spatial patterns of biodiversity composition, the BHI can reveal locations where the impact of habitat degradation on biodiversity persistence has been greatest owing to their ecological uniqueness. While panel c) reveals the moderating effect of terrain in enhancing resilience on mountain sides where species can track shifting climates up-slope, the present-day climates at mountain tops are expected to disappear, and so BERI values considerably decline in these locations. Meanwhile, climate velocity will generally be greater in the flatter lowlands, requiring species to move further to track suitable climates, leading to lower levels of resilience. PARC indices are shown in panels c-d) revealing the degree to which protected areas and OECMs represent the biological diversity of the Dominican Republic (panel c), and the degree to which these areas are connected to each other and to other areas of intact habitat (panel d). Borders of protected areas are depicted on these maps as dashed black lines.

Supporting Information

Appendix S1: Extended methods

Overview

The methods described are for four biodiversity indicators: the Biodiversity Habitat Index (BHI); the Bioclimatic Ecosystem Resilience Index (BERI); the Protected Area Representativeness and Connectedness Index for representativeness (PARC-representativeness); and the Protected Area Representativeness and Connectedness Index for connectivity (PARC-connectedness). Calculation of these indicators uses the following key input data, in different combinations (Table S1):

- Spatial layers representing predictions from a generalized dissimilarity model (GDM) of the difference in species composition expected between ecological communities at any two locations (30 arcsecond grid-cells) on the planet under current climatic conditions
- Spatial layers representing predictions from a GDM of differences in species composition expected under alternative future climate scenarios
- A spatial layer representing the estimated annual ecosystem condition for each location
- A spatial layer representing the estimated annual connectivity-adjusted ecosystem condition for each location
- Spatial data (shapefile or raster) representing the annual coverage of protected areas

Table S1.1. The key inputs to the calculations for each of the biodiversity indicators.

Key inputs	BHI	BERI	PARC-representativeness	PARC-connectedness
GDM prediction layers: present climate	✓	✓	✓	
GDM prediction layers: future climate		✓		
Ecosystem condition layer		✓		✓
Connectivity-adjusted ecosystem condition layer	✓			
Spatial data on coverage of protected areas			✓	✓

The biodiversity indicators can be applied using inputs derived for any analysis region of interest, such as for individual countries. The methods and data presented here relate to the generation of the four biodiversity indicators for all terrestrial areas globally (excluding Antarctica) at ≈1 km (30 arcsecond) spatial resolution at an annual timestep for the period 2000-2024. These global data can be used to derive indicator summary values for any user-defined spatial reporting area.

The methods detailed below (Figure S1) build on, and refine, those described in previous data publications and applications of these indicators (Di Marco, Ferrier, et al. 2019; Ferrier et al. 2020, 2024; Harwood et al. 2022; Hoskins et al. 2020; Marco et al. 2019). These refinements relate particularly to improving the computational simplicity and efficiency of the global implementation of the indicator calculations by: (i) employing a single GDM across all taxa in each biogeographic realm; and (ii) summarising the continuous GDM spatial predictions using a discrete classification.

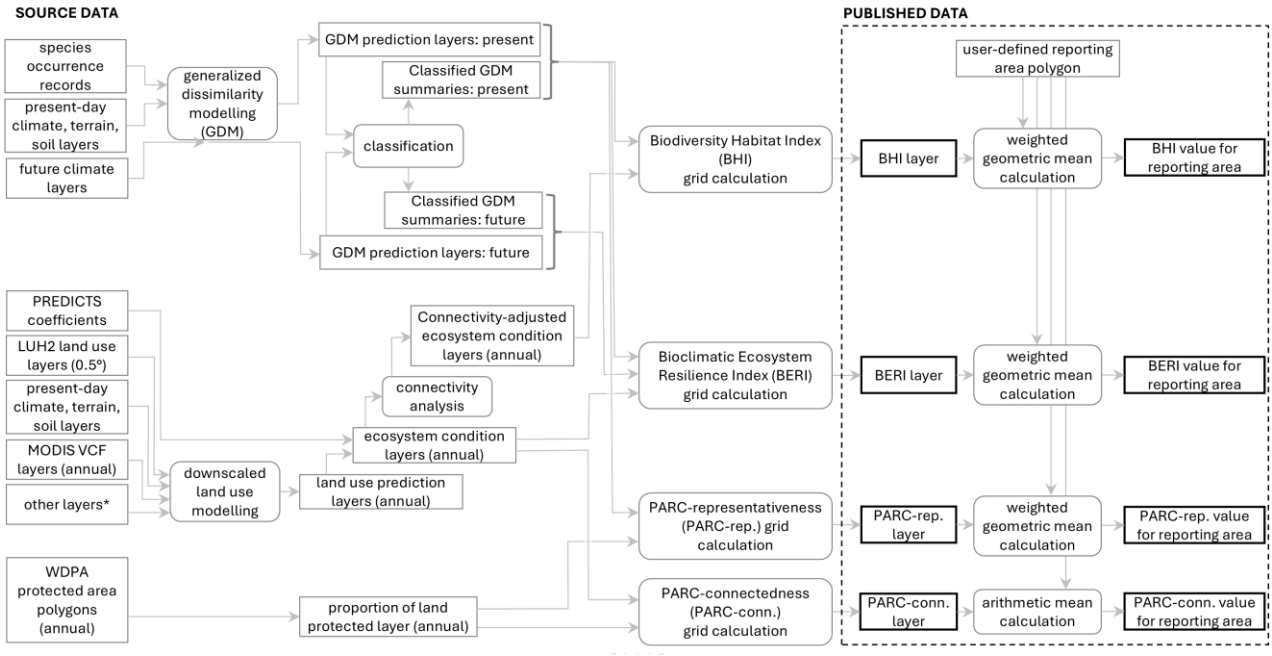

Figure S1.1. A conceptual overview of the analytical approach to developing the biodiversity indicators for the global terrestrial land surface (excluding Antarctica). Methodological details of each component are provided below. * Other layers include gridded population data and annual land cover data, as described below.

Data inputs

Biodiversity models

Previous global applications of these biodiversity indicators used global models of spatial turnover in species composition of ecological communities developed by Hoskins et al. (2020) for three broad taxonomic groups: vertebrates, invertebrates, vascular plants, with 49 separate models for each group nested within biome and realm combinations (Olson et al. 2001) (i.e. 146 models in total). As described in Hoskins et al. (2020), those models were fitted using >100M species-occurrence observations downloaded from GBIF covering >400,000 species across these three taxonomic groups. Those models were fitted using 17 spatial environment layers as predictors, including seven soil variables, two topographic variables and eight climate variables (Hoskins et al. 2020).

To provide greater computational efficiency and simplicity in calculating the biodiversity indicators globally, we generalised the models presented by Hoskins et al. (2020) to a single model for each realm (i.e. seven models total) that describe and predict patterns of compositional turnover for all three taxonomic groups combined (vertebrates, invertebrates and vascular plants) across all biomes within a realm. The objective was to generalise the existing models rather than to fit new models to the source species-occurrence data, so as to retain coherence with previous global applications of the indicators. For each realm, we therefore generated site-pair predictions of compositional dissimilarity from the models of Hoskins et al. (2020), for each combination of taxonomic group and biome within that realm. We then fitted new GDMs using these predicted dissimilarities as the response variable, and the same suite of 14 spatial environmental layers (Hoskins et al. 2020) as the predictor variables.

Site pairs employed in the model simplification were selected using a feature-space-coverage sampling approach (Brus 2019), to ensure that the set of samples were representative of the multivariate space defined by the set of predictor variables. The geographic distance between the sites in a pair was used to further refine the selected site pairs, ensuring adequate sampling of site pairs exhibiting different levels of geographic separation. For each site pair selected, the predicted dissimilarities from the separate models

for each taxonomic group were derived (see Table S1.2 for the number of site pairs used per realm). These site-pair dissimilarities were then combined and used to fit a single all-taxa GDM for each realm, using the 14 spatial environmental layers from Hoskins et al. (2020) plus geographic distance. The accuracy of the simplified GDM for each realm in representing the multiple biome and taxa GDMs for that realm, from Hoskins et al. (2020), was tested using an independent set of site pairs (Table S1.2). It should be noted that given the simplified realm models are synthesising predictions from many component models, it is impossible for these single realm-wide all-taxa models to recreate predictions of the component models perfectly.

Table S1.2. Attributes and performance metrics for the 7 realm-wide all taxa models used to summarise and generalise the 146 models from Hoskins et al. (2020).

Realm	Land area (M km^2)	No. of biomes	Original no. of models	No. of site pairs: train	Deviance explained (%)	intercept	No. of site pairs: test	Mean error	Mean absolute error	Root mean square error
Australasia	9.2	9	26	624,111	80.2	0.04	89,113	0.000	0.057	0.078
Afrotropics	21.7	8	24	709,143	81.0	0.02	171,281	0.000	0.056	0.073
Indo-Malaya	8.5	9	27	820,004	80.2	0.01	109,943	0.000	0.060	0.077
Nearctic	20.5	10	30	530,823	88.0	0.00	178,215	0.000	0.041	0.057
Neotropics	19.3	10	30	887,145	83.9	0.04	193,806	0.000	0.045	0.061
Oceania	0.05	3	9	567,417	55.0	0.00	1,863	0.000	0.108	0.150
Palearctic	52.8	10	30	631,959	65.5	0.03	335,511	0.000	0.089	0.119

The seven simplified GDMs (one per realm) were used to generate spatial prediction layers for both 'current' climate (1960–1900 period) (Hijmans et al. 2005) and six climate scenarios centred on 2050 from downscaled CMIP5 climate projections accessed through WorldClim (https://worldclim.org). These climate scenarios include four representative concentration pathways (RCPs) under the IPSL-CM5A-LR general circulation model (GCM) (2.6, 4.5, 6.0, 8.5), and an additional two GCMs under RCP 8.5: ACCESS1-0 and GFDL-CM3 (as per Ferrier et al. (2020)).

Classifying realm-wide biodiversity models

To improve the computational efficiency of the biodiversity indicator calculations, the GDM spatial prediction layers for each biogeographic realm for the current climate, were used to derive classes of cells with high predicted compositional similarity to one another. For each set of GDM prediction layers, a two stage classification approach was implemented using *k*-means classification (Ikotun et al. 2023) with mini-batch implementation within the python package scikit-learn (Pedregosa et al. 2011). This involved a first round of classification by k-means, followed by a second-round reclassification for those 25 % of classes with the lowest within-class median compositional similarity between pairs of grid cells. In the second round of classification, the number of classes was allowed to be double that of the number in the 25 % of all classes that were being reclassified.

The number of classes per realm was determined by generating a range of potential numbers of initial classes (1,000; 2,000; 3,000; 5,000; 10,000; 15,000; 20,000) and selecting the smaller number of classes which produced a final within-class median predicted compositional similarity between pairs of grid cells within a class of 0.87 or slightly higher (Table S1.3). Other parameters of the k-means classification were set based on best available information and experimentation, being applied consistently across all realms (*n_init* = 51; *max_iter* = 1,500; *batch_size* = 10,000; *tol* = 1e-6; *random_state* = 42; *reassignment ratio* = 0.0005) (Pedregosa et al. 2011).

Table S1.3. Attributes and performance metrics of the classification of the GDM prediction layers for each of the seven realm-wide all taxa models. The initial number of classes is that applied at the commencement of the first stage of the classification, and the final number of classes is that at the completion of the second stage of the classification.

Realm	Initial number of classes	Final number of classes	Median within class cell-pair similarity
Australasia	5,000	7,496	0.88
Afrotropics	10,000	14,981	0.89
Indo-Malaya	10,000	14,972	0.87
Nearctic	10,000	15,000	0.87
Neotropics	20,000	29,906	0.87
Oceania	1,000	1,000	0.91
Palearctic	3,000	4,500	0.87

For each classified realm, the class centroid values for each of the 16 GDM prediction layers (one per environmental predictor and two for geographic distance) for each class were obtained, along with a spatial layer indicating the class membership of every grid cell.

Ecosystem condition - overview

A spatial layer estimating ecosystem condition for a given time point is an important input to three of the four biodiversity indicators (Table S1). Ecosystem condition represents the capacity of an area to maintain its characteristic composition, structure, functioning and self-organization over time within a natural range of variability (United Nations 2024). In the current application, ecosystem condition ranges continuously from 0 to 1, where a value of '1' would be associated with a location of intact primary vegetation in pre-industrialised reference condition, and a value of '0' would be associated with an area that is completely degraded and has no value for biodiversity. A condition value of '0.5' would be associated, at least conceptually, with an area (e.g. grid cell) that is 50 % covered by primary vegetation and 50 % covered by completely degraded land.

The approach we applied to derive a spatial layer of ecosystem condition for each time point has been described in (Di Marco, Harwood, et al. 2019) (section 2.2). In summary, for each year (2000–2024) we first estimated the proportion of each ≈1 km grid cell occupied by each of the 12 land-use classes in version 2 of the land-use harmonisation dataset (LUH2) (Hurtt et al. 2020). We then apply coefficients derived from a model fitted using the PREDICTS database (Hudson et al. 2017) to convert the proportional land-use coverage estimates into annual estimates of ecosystem condition. The methods implemented for both these steps are described below.

Ecosystem condition – estimating proportional coverage of land-use classes

Annual estimates (2000–2024) of the proportion of each ≈1 km (30-arcsecond) grid cell occupied by each of the 12 land use classes were derived through statistical downscaling followed by algorithmic adjustments based on ancillary data, with refinements to previously published methods (Hoskins et al. 2016; Marco et al. 2019). The statistical downscaling approach uses generalized additive modelling and constrained optimisation fitted to the LUH2 spatial data for 2015 (≈25 km resolution) (Hoskins et al. 2016). This fitted model is then used to predict the proportional coverage of all 12 LUH2 land-cover classes at ≈1 km resolution for each year from 2000 to 2024. The downscaling covariates used in model fitting, and for generating annual predictions, include eight static spatial environmental layers (soil, topography, climate) and the following dynamic predictors, resampled to the resolution of the downscaled land use data (≈1 km): (i) annual time series (2000–2024) of MODIS v6.1 Vegetation Continuous Fields (VCFs) (DiMiceli, Sohlberg, and Townshend 2022); (ii) annual land-cover data for urban areas from the European Space Agency's Climate Change Initiative (ESA-CCI) (ESA 2017); (iii) annual population density from the

Gridded Population of the World, Version 4 (CIESIN 2018), where values for years (t) between 5-yearly values (y) were estimated using an exponential model ($\log(y) \sim t$) fitted to the available years of data for each grid cell.

A series of algorithmic adjustments were then performed to the statistical downscaling predictions of the proportional coverage of each of the 12 LUH2 land-cover classes in each ≈1 km grid cell, including: (i) a cropping adjustment; (ii) a primary-vegetation adjustment; and (iii) a total-proportion adjustment.

For the cropping adjustment, annual land-cover data from the ESA-CCI (ESA 2017) were resampled from 300 m to the resolution of the downscaled land-use data (≈1 km). For each year and grid cell, the downscaled proportions of each of the LUH2 cropping classes (c3 nitrogen fixing, c3 perennial, c4 perennial, c3 annual, c4 annual) were adjusted so that they summed to the total proportion of the cell covered by cropping in that year according to the ESA-CCI dataset. The adjustments were made so that the relative proportions of the statistically downscaled cropping classes were maintained. Given the ESA-CCI data available at the time of analysis were for the years 1990-2022, the 2022 ESA-CCI values for each grid cell were applied for the years 2023 and 2024.

The primary-vegetation adjustment aimed to minimise any increases in the proportion of a grid cell covered by the primary vegetation land-use classes (primary forest, primary non-forest). Increases in primary vegetation conflicts with the LUH2 definitions of primary vegetation (Hurtt et al. 2020); however, there is no mechanism in the statistical downscaling to prevent increases over time. Hence, we inferred that increases in the proportion of primary forest estimated by the statistical downscaling should be allocated instead to the proportion of secondary forest, and similarly for primary and secondary non-forest.

The final adjustment undertaken was simply to ensure that the sum of the proportional coverage of all LUH2 land use classes in a grid equals exactly '1.0', accounting for floating point precision error in the above statistical downscaling and subsequent adjustments. Hence, the proportional coverage values of all LUH2 land-use classes were scaled so that they retain their relative proportions but summed to exactly '1.0'.

Ecosystem condition – converting land use to ecosystem condition using PREDICTS

The spatial layers estimating the proportional coverage of each LUH2 land-use class in each ≈1 km grid cell were converted to ecosystem condition by applying coefficients specifying the expected condition, on average, of ecosystems falling within each land-use class (Table S1.4). These ecosystem-condition coefficients were themselves derived from the estimated fraction of naturally-present species expected to persist in spite of land-use change. As shown by (Newbold et al. 2016), this fraction can be estimated as the product of two quantities, each of which can be modelled using the PREDICTS global database (Hudson et al. 2014): within-sample species richness (relative to that in primary vegetation) and species-based compositional similarity to a primary-vegetation site. For the present study, data for modelling were derived from an extract of the PREDICTS database from 22nd March 2024, consisting of 33,261 sites from 911 studies in 102 countries. Each site's taxon richness was calculated as the number of named taxa recorded during sampling, with each study placed into one of nine taxonomic groupings (Coleoptera, Hymenoptera, other insects, other arthropods, other invertebrates, birds, other vertebrates, dicots, others – subdividing the database roughly equally) based on which had most named taxa. Prior to modelling, the PREDICTS sites were also classified into the land-use classes listed in Table S1.4, though some classes were pooled for modelling to ensure sufficiently large sample sizes.

Species richness relative to sites in primary vegetation was modelled as a function of land use, by fitting a zero-inflated negative binomial GLMM using the *glmmTMB* package in R (Brooks et al. 2017). The model also included taxonomic imprecision as a control variable, and nested random intercepts for taxonomic grouping, study and spatial block. The species-based compositional similarity between each primary-

vegetation site and every other site (which could be of any land use including primary) within the same study was calculated as the fraction of species present at the primary site that were also present at the other site (an asymmetric version of the Jaccard index: Newbold et al. 2016). This fraction was modelled as a function of land use by fitting a a binomial GLMM, again using the *glmmTMB* package. In addition to the same control variables and random intercepts included in the modelling of species richness, this model also included control variables for geographic and environmental distances between sites.

The PREDICTS analysis estimated the proportion of native species remaining in a land-use class (l) relative to reference condition (α_l). In contrast, the definition of ecosystem condition (h_l) that we assume in deriving our biodiversity indicators equates to the equivalent area of habitat remaining under a land-use class (A_l) relative to reference (A_{ref}):

$$h_l = \left(\frac{A_l}{A_{ref}}\right) \quad \text{Equation 1}$$

It is therefore necessary to convert the PREDICTS-estimated proportion of native species remaining to an area-equivalent ecosystem condition estimate (h_l). This conversion needs to account for the non-linear species-area scaling of the proportion of species remaining under a land-use class to the equivalent area of habitat under that land-use class (Ferrier et al 2024), for which we apply a power-law species-area relationship:

$$\alpha_l = \left(\frac{A_l}{A_{ref}}\right)^z \quad \text{Equation 2}$$

where we use a value for the species-area exponent (z) of 0.25, as observed and applied widely by others (García Martín and Goldenfeld 2006; Rosenzweig 1995). The estimated condition under a given land-use can then be derived from the estimated remaining under that land-use:

$$h_l = \left(\frac{A_l}{A_{ref}}\right) = {\alpha_l}^{1/z} \quad \text{Equation 3}$$

which simplifies to $h_l = \alpha_l^4$ when z = 0.25. This approach was applied to convert the PREDICTS-derived proportion of native species remaining to ecosystem condition equivalents (Table S1.4).

Ecosystem condition for a given grid cell in a given year was then derived as a weighted arithmetic mean of the 12 h_l values (one for each LUH2 land-use class) with weights set to the estimated proportional coverage of each land-use class within that cell.

Table S1.4. Estimated proportion of native species remaining in each land use class to primary vegetation, and the associated estimated ecosystem condition for each land use class.

LUH2 land use class	PREDICTS land use class	Proportion of native species remaining (PREDICTS)	Ecosystem condition
Primary forest	Primary vegetation	1	1
Primary non-forest	Primary vegetation	1	1
Secondary forest	Secondary vegetation	0.810	0.430
Secondary non-forest	Secondary vegetation	0.810	0.430
Rangelands	Rangelands	0.776	0.363
Urban*	Urban	0	0
Managed pasture	Managed Pasture	0.396	0.025
c3 perennial crops	Perennial croplands	0.426	0.033
c4 perennial crops	Perennial croplands	0.426	0.033
c3 annual crops	Annual croplands	0.432	0.035
c4 annual crops	Annual croplands	0.432	0.035
c3 N-fixing crops	Annual croplands	0.432	0.035

*- for urban areas a value of 0 is applied

Ecosystem condition – deriving connectivity-adjusted condition

To derive the BHI indicator, the ecosystem condition layer for each year is further adjusted to account for the effects of connectivity to areas of habitat in the neighbourhood around each pixel. This connectivity-adjusted ecosystem condition layer is created using an extension of the cost-benefit approach (CBA) developed by (Drielsma, Ferrier, and Manion 2007) which is based on principles of meta-population ecology.

For enhanced computational efficiency, our implementation of the CBA landscape connectivity analysis uses multi-resolution overviews embedded in the GeoTIFF file representing the ecosystem condition data. This file stores average condition values for progressively coarser-resolution square blocks comprised of dimensions 2, 4, 8, 16 and 32 grid cells. Nodes representing the neighbourhood around each grid cell i are configured based on the multi-resolution overviews (e.g. Figure S1).

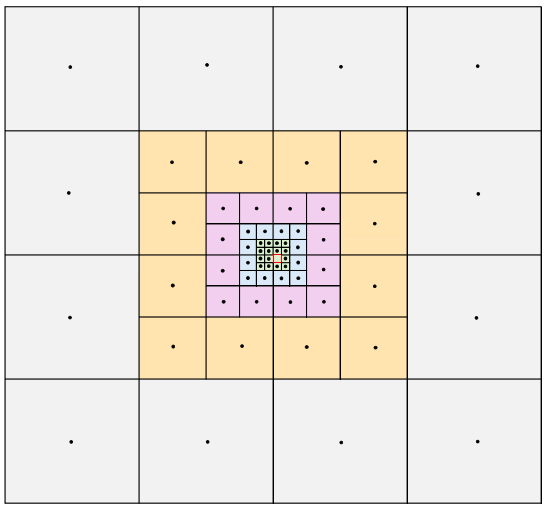

Figure S1.2. Representation of the multi-resolution neighbourhood approach applied in the connectivity analyses. The focal grid cell (i) is shown in red in the centre, with nodes (black dots) in the centre of each grid cell (at the different resolutions). The above example uses four cells wide at each resolution for demonstration purposes, whereas our analysis applied 11 cells wide at each resolution, resulting in a maximum neighbourhood radius of 352 km around each focal cell.

All the nodes in the multi-resolution neighbourhood around each focal grid cell i are used to construct a directed weighted graph, with edges created between each node g and its immediate neighbour nodes. The condition-weighted length of each edge (D_q), i.e. the condition weighted distance between the two nodes it connects, is:

$$D_q = L_q\big(h_q(1 - M) + M\big) \qquad \text{Equation 4}$$

with L_q being the length of edge q (i.e. the haversine distance in kilometres between the connected nodes), h_q being the average ecosystem condition at the head node (destination node) of the edge q (on a 0–1 scale), and m being the scalar for the degree to which low ecosystem condition increases the cost to movement. In the current application we apply M = 2, meaning that an area with the lowest ecosystem condition (h_q = 0) is twice as difficult to move through compared to an area in the highest condition (h_q = 1).

For node g, the condition weighted distance of the least cost path (d_{ig}) from the focal grid cell i through all the n_{edge} intervening edges q in the graph is calculated as the Dijkstra shortest path:

$$d_{ig} = \sum_{q=1}^{n_{edge}} D_q$$ Equation 5

which is used to determine the link permeability from focal cell i to node g (K_{ig}) (Drielsma et al. 2007) by incorporating the condition weighted least-cost path distance (d_{ig}) into a dispersal kernel, for which we use a simple negative exponential:

$$K_{ig} = \mathrm{e}^{-d_{ig}/\lambda}$$ Equation 6

For the median dispersal distance (λ), we apply three values to reflect the different movement abilities of various taxa (λ = 2, 20 and 200 km).

The degree to which node g offers connected habitat to the focal cell i (H_{ig}) is calculated by multiplying the link permeability to node g with the average ecosystem condition value of node g (h_g), adjusting for the number of valid grid cells represented by node g (n_g):

$$H_{ig} = K_{ig} h_g n_g$$ Equation 7

The total connected habitat (Γ_i) to focal cell i, from all N nodes in the multi-resolution neighbourhood is the sum of the connected habitat to each node (Drielsma et al. 2007):

$$\Gamma_i = \sum_{g=1}^{N} H_{ig} = \sum_{g=1}^{N} K_{ig} h_g n_g$$ Equation 8

The relative amount of total connected habitat to focal cell i ($\Gamma_{i,rel}$) is the total connected habitat as a proportion of the maximum possible total connected habitat ($\Gamma_{i,max}$), assuming all cells in the surrounding neighbourhood have the highest possible ecosystem condition and the least-cost paths connecting these cells to the focal cell are recalculated accordingly:

$$\Gamma_{i,rel} = {\Gamma_i}/{\Gamma_{i,max}}$$ Equation 9

The relative amount of total connected habitat to focal cell i is averaged across the results for the three alternative median dispersal distances applied above (λ = 2, 20, 200 km). Finally, the connectivity-adjusted ecosystem condition value for focal cell i ($h_{i,con}$) is derived as the geometric mean of the ecosystem condition of focal cell i (h_i) and the relative amount of total connected habitat:

$$h_{i,con} = \sqrt{h_i \Gamma_{i,rel}}$$ Equation 10

Protected areas

For the PARC-representativeness and PARC-connectivity indicators, a key input is a spatial grid representing the proportion of the land in each grid cell that is covered by a protected area or other effective area-based conservation measure (PA+OECM) in a given year. Data delineating the boundaries of terrestrial PA+OECM were obtained from the World Database on Protected Areas (WDPA) (IUCN-WCMC 2025) on 20 November 2025. For each year assessed (2000-2024) all terrestrial PA+OECMs established prior to the end of that year were selected. Marine protected areas were filtered out by only considering PA+OECMs that intersected with the land mask used for our analyses. PA+OECMs were further filtered to remove those regions which had the status ("STATUS" field) designation of "proposed." The WDPA and WDPA+OECM databases include both polygons depicting the boundaries of PA+OECMs and, separately, points

representing PA+OECM centroids where polygons are either not available or are too small to be represented by a boundary (e.g. an individual tree or nesting site). We opted to exclude the latter (7,937 points) from our analyses as there is no way to ascertain the shape (and in many cases the size) of the corresponding the PA or OECM. For our analyses, we translated the PA+OECM data to our analysis land mask by calculating the proportion of each grid cell covered by PA+OECMs. Proportions were calculated by rasterising the PA+OECMs using a super sampling method: PA+OECM geometries were rasterised to a grid 10 times higher than the resolution of the analysis land mask, and then aggregated to the analysis resolution (≈1 km) by averaging the super sampled pixels. This produces a grid with values approximating the proportion covered by protected areas. Finally, the proportion of land within each grid cell covered by PA+OECMs was determined by dividing the proportion of each ≈1 km grid cell covered by PA+OECMs by the proportion of each grid cell covered by land.

Country-level reporting areas

To summarise biodiversity indicator results for each country, we used country boundaries from the Database of Global Administrative Areas (GADM 2024). We also summarised each indicator by the intersection of biomes and countries using biome boundaries from (Olson et al. 2001).

Indicator calculation

The Biodiversity Habitat Index (BHI)

The Biodiversity Habitat Index (BHI) estimates the level of species diversity expected to be retained within any given spatial reporting unit (e.g. a country, a biome, an ecosystem type, or the entire planet) as a function of the area, condition and connectivity of natural ecosystems across that unit. Results for the indicator are expressed as the proportion of species in the reporting unit expected to persist (i.e. the proportion expected to avoid extinction) over the long term.

Based on the standard formulation of this approach (e.g. (Allnutt et al. 2008; Ferrier et al. 2024; Marco et al. 2019; Mokany et al. 2020)) the foundational calculation for deriving the BHI for each grid cell i is simply:

$$BHI_i = \left[\frac{\sum_{j=1}^{n} s_{ij} h_{j,con}}{\sum_{j=1}^{n} s_{ij}}\right]^z \qquad \text{Equation 11}$$

where s_{ij} is the predicted compositional similarity (if all cells were still in perfect condition) between the focal grid cell i and each of the n other grid cells j, $h_{j,con}$ is the connectivity-adjusted ecosystem condition of grid cell j (on a 0–1 scale), and z is the exponent of the species-area relationship, for which we employ the widely adopted value of z = 0.25 (Rosenzweig, 1995). BHI calculations are performed within biogeographic realms (Olson et al. 2001), such that a given focal cell is compared to all other grid cells in the biogeographic realm. While we recognise that realm boundaries are porous to some extent, constraining calculations in this way accounts for the overarching effects of biogeographic history in shaping broader biodiversity patterns.

For the present implementation, we incorporated two enhancements to the above approach. The first of these relaxes an assumption inherent in the standard formulation – i.e. that all species originally associated with the focal cell i (prior to any loss of condition of habitat within that cell) will share an equal probability of originally occurring in any other cell j, with that probability being equal to s_{ij}, the declining compositional similarity between cells i and j as these two cells are increasingly separated spatially and environmentally. In reality, the species originally associated with cell i are likely to vary in the breadth of their environmental niches – ranging from more specialised narrow-niche species occurring only in environments highly similar to that cell, through to generalist species occurring more broadly across

environments exhibiting lower levels of similarity to the focal cell. To better accommodate this likely reality, we extend the basic approach presented in Equation 11 by further treating s_{ij} as an estimate of the proportion of species associated with focal cell i that are expected to have an environmental niche wide enough to also include cell j. For example, a cell with a predicted similarity of 0.9 is assumed to fall within the niche of 90 % of the species associated with the focal cell, while a cell with a similarity of 0.1 will fall within the niche of only 10 % of those species.

To extend the species-area calculation from Equation 11 to incorporate this assumption, we adopt an iterative approach modelled on that proposed by (Drielsma et al. 2014).

This involves calculating BHI for cell i using r (in this case 20) evenly spaced bins b of compositional similarity between 0 and 1:

$$BHI_i = \frac{1}{r}\sum_{b=1}^{r}\left[\frac{\sum_{j=1}^{n} s_{ij} h_{j,con}}{\sum_{j=1}^{n} s_{ij}}, s_{ij} > s_b\right]^z \quad \text{Equation 12}$$

where s_b is the lower similarity limit for bin b.

To make the BHI calculations computationally tractable at a global scale, we implemented a second modification to the foundational calculation. We replace n grid cells j in the calculation with n cluster centroids j derived from the classified global GDMs. Given cluster centroids should represent cluster member cells well, this is a reasonable short-cut in computing the compositional similarities (s_{ij}). To ensure all connectivity-adjusted ecosystem condition values ($h_{j,con}$) for grid cell j are represented, we compute the sum of condition values associated with each cluster. This summed condition then becomes the $h_{j,con}$ value used to scale similarity s_{ij}. To ensure the denominator term is balanced, denominator s_{ij} values are multiplied by the number of grid cells each cluster centroid represents. We use cluster centroids in the manner described above to represent all grid cells which don't fall in the same cluster as a focal grid cell. Where a focal grid cell is to be compared to the centroid of the cluster for which the cell itself is a member, we revert to individual cell-to-cell comparisons. We have found that this hybrid approach effectively balances computational efficiency resulting from the use of discrete classes with the rigour of working with continuous data in regions of habitat which are likely to be most compositionally similar to a given focal cell.

To derive a BHI value for any larger reporting region (BHI_r) such as a country, a weighted geometric mean is taken of the BHI_i values of all R grid cells i falling within that reporting region (Ferrier et al. 2024; Marco et al. 2019):

$$BHI_r = \exp\left[\frac{\sum_{i=1}^{R} w_i \ln(BHI_i)}{\sum_{i=1}^{R} w_i}\right] \quad \text{Equation 13}$$

where the contribution of each cell is weighted (w_i) by the predicted similarity (overlap) in species composition between this cell i and all n other cells j globally, and therefore its ecological uniqueness:

$$w_i = \frac{1}{\sum_{j=1}^{n} s_{ij}} \quad \text{Equation 14}$$

Given that compositional similarity and connectivity-adjusted ecosystem condition in all other grid cells j globally are used in estimating the BHI value for each grid cell i, the BHI value for a larger reporting region will be influenced to some degree by changes in connectivity-adjusted ecosystem condition outside that region. While this reflects the best estimate of persistence expected for species associated with the region of interest, anywhere across the broader range of those species, it may be desirable for some reporting purposes to derive BHI values for a reporting region by treating that region as a closed system (BHI_c), or in

other words to constrain the grid cells j with which each focal cell is compared, in all the above equations, to only those cells falling within the region of interest. We used this approach to calculate closed-system BHI results for all countries, which is reported alongside the standard BHI (i.e. open-system) value for each country. Because the closed-system formulation imposes an artificial boundary on the extent of possible habitat that may be included in any calculation, its value lies only in the capacity to identify changes in the BHI resulting wholly from changes to ecosystem condition within a region of interest. In this way, it lends itself to monitoring outcomes of management within discrete regions, and for this reason, we supply this formulation of the BHI only for countries.

The Bioclimatic Ecosystem Resilience Index (BERI)

The Bioclimatic Ecosystem Resilience Index (BERI) assesses the capacity of landscapes to retain species diversity in the face of climate change, as a function of the area, condition and connectivity of natural ecosystems across those landscapes. The indicator assesses the extent to which any given spatial configuration of natural habitat will promote or hinder climate-induced shifts in biological distributions. It does this by analysing the functional connectivity of each grid-cell of natural habitat to areas of habitat in the surrounding landscape which are projected to support a similar assemblage of species under climate change to that currently associated with the cell of interest.

The broad approach to calculating the BERI has been described previously (Ferrier et al. 2020; Harwood et al. 2022), and here we follow the same approach, with minor modifications. For the derivation of BERI presented here, we apply the same representation of the landscape surrounding a focal grid cell i as described for the connectivity-adjusted ecosystem condition analysis described above (Figure S1.2). Hence a multi-resolution gridded neighbourhood around cell i is used to construct a directed weighted graph, where each node j represents a neighbouring grid cell at a given resolution, with each node connected by edges to its immediate neighbour nodes (Figure S1.2).

The amount of accessible connected habitat in the landscape surrounding grid cell i which is projected to support a similar assemblage of species under climate scenario k to that currently associated with focal cell i is calculated as:

$$C_{ik} = \sum_{j=1}^{n} \left(K_{ij}\, h_j n_j\, s_{ijk} \right) \qquad \text{Equation 15}$$

where K_{ij} is the link permeability (Drielsma et al., 2007) from the focal cell i to each of the n nodes j, h_j is the average ecosystem condition of node j , n_j is the number of valid grid cells represented by node j and s_{ijk} is the expected compositional similarity between the focal cell i under present-day climate and node j under climate scenario k if both i and j were in reference condition (Ferrier et al. 2020; Harwood et al. 2022). The connectedness metric C_{ik} was calculated separately for each of the six future climate scenarios described above as well as for the current climate.

For the link permeability (K_{ij}) from focal cell i to node j in Equation 15, we apply a gaussian dispersal kernel to the condition weighted least-cost path distance (d_{ij}) (Equation 5) to account for the broader movement potential of species populations over the scale of many years (t) (Harwood et al. 2022):

$$K_{ij} = \exp\left[-\frac{\left(\frac{d_{ij}}{\lambda}\right)^2}{ut} \right] \qquad \text{Equation 16}$$

where we employ t = 50 years, given this is the approximate interval between the base climate and the climate change scenarios, and for the constant we employ u = 5.8. As with the connectivity-adjusted

ecosystem condition (Equation 6), we apply three alternative median dispersal distances (λ = 2, 20 and 200 km).

For each median dispersal distance, the BERI value for the focal cell i ($BERI_{i,\lambda}$) is summarised across all the m climate scenarios using the limited degree of confidence approach (McInerney, Lempert, and Keller 2012), which averages the minimum and mean connectivity values across the scenarios:

$$BERI_{i,\lambda} = \frac{0.5\left(\frac{\sum_{k=1}^{m} C_{ik}}{m} + min\{C_{i1}, \dots, C_{im}\}\right)}{C_{i0}} \quad \text{Equation 17}$$

where C_{i0}, is the maximum possible connectivity value, obtained by assuming the focal cell is completely surrounded by a continuous expanse of habitat in perfect condition, with no change in climate. The BERI value for each grid cell is then derived by averaging the scores obtained using all v median dispersal distances:

$$BERI_i = \frac{1}{v}\sum_{\lambda=1}^{v} BERI_{i,\lambda} \quad \text{Equation 18}$$

As for the BHI indicator, to derive a BERI value for any larger reporting region ($BERI_r$) such as a country, a weighted geometric mean is taken of the $BERI_i$ values of all R grid cells i falling within that reporting region:

$$BERI_r = \exp\left[\frac{\sum_{i=1}^{R} w_i \ln(BERI_i)}{\sum_{i=1}^{R} w_i}\right] \quad \text{Equation 19}$$

where the contribution of each cell is weighted (w_i) by the predicted similarity (overlap) in species composition between this cell i and all n other cells j globally, and therefore its ecological uniqueness (Equation 14).

Again, as for the BHI indicator, for every country we also calculate BERI values treating the country as a closed system ($BERI_c$) – hence, in all the above equations, comparing each focal cell i only with those other grid cells j falling within that country. This closed-system BERI value is reported alongside the standard (i.e. open system) BERI value for each country.

The Protected Area Representativeness and Connectedness Index for representativeness (PARC-representativeness)

The PARC-representativeness index quantifies the extent to which a system of terrestrial protected areas and OECMs is ecologically representative of the full range of environmental and biological diversity present within any given spatial reporting unit (e.g. a country). PARC-representativeness scores are initially calculated separately for each and every grid-cell (both protected and unprotected) within the spatial domain of interest. For each cell i, PARC-representativeness estimates the proportional protection of all cells that are ecologically similar to that cell – i.e. the proportion of all ecologically-similar cells that are included in the protected-area system.

Specifically, the PARC-representativeness value for each grid cell i ($PARCrep_i$) is derived as:

$$PARCrep_i = \frac{\sum_{j=1}^{n} s_{ij} p_j}{\sum_{j=1}^{n} s_{ij}} \quad \text{Equation 20}$$

where s_{ij} is the predicted compositional similarity between the focal grid cell i and all n other grid cells j, and p_j is the proportion of land covered by protected areas and OECMs in grid cell j. We incorporate the same enhancements in deriving PARC-representativeness as those adopted in deriving the BHI. That is, we

extend the standard calculation of $PARCrep_i$ presented in Equation 20 through adoption of the binning approach described in Equation 12, although in this case the estimated proportions of land protected are not raised to the power of the species-area exponent z. We also, again, improve computational efficiency by using cluster centroids resulting from the GDM classification to represent compositionally similar grid cells.

As for the BHI and BERI indicators, to derive a PARC-representativeness value for any larger reporting region r ($PARCrep_r$), such as a country, a weighted geometric mean is taken of the $PARCrep_i$ values of all R grid cells i falling within that reporting region:

$$PARCrep_r = \exp\left[\frac{\sum_{i=1}^{R} w_i \ln(PARCrep_i)}{\sum_{i=1}^{R} w_i}\right] \quad \text{Equation 21}$$

where the contribution of each cell is weighted (w_i) by the predicted overlap in species composition between this cell i and all n other cells j globally, and therefore its ecological uniqueness (Equation 14).

Again, as for the BHI and BERI indicators, for every country we also calculate PARC-representativeness values treating the country as a closed system ($PARCrep_c$) – hence, in all the above equations, comparing each focal cell i only with those other grid cells j falling within that country. This closed-system PARC-representativeness value is reported alongside the standard PARC-representativeness (i.e. open system) value for each country.

The Protected Area Representativeness and Connectedness Index for connectedness (PARC-connectedness)

The PARC-connectedness index provides a measure of the extent to which protected areas and OECMs are functionally connected to one another and to other areas of intact natural ecosystems, thereby enhancing integration into the wider landscape. The PARC-connectedness value reflects the connectedness of a set of protected areas to each other and to unprotected natural vegetation in the surrounding landscape. The PARC-connectedness score assigned to each protected cell is expressed as a proportion (0 to 1) of the maximum possible level of connectedness obtainable if that cell were surrounded by a continuous expanse of protection, or otherwise natural vegetation in the surrounding landscape.

PARC-connectedness scores are calculated for each grid-cell i that have a non-zero proportion of land covered by protected areas and OECMs (p_i).

For the derivation of PARC-connectedness presented here, we use the same method as applied for the connectivity-adjusted ecosystem condition analysis described above (Equation 4 –Equation 9). The key difference is that for the PARC-connectedness analysis, the proportion of land protected in each grid cell (p_i) is combined with the ecosystem condition of each grid cell (h_i) in deriving a value for the "protected-condition" (ϕ_i), by taking the maximum of p_i and h_i for each cell i:

$$\phi_i = \max(p_i, h_i) \quad \text{Equation 22}$$

The relative amount of total protected-connected habitat to focal cell i ($\Gamma_{i,rel}$) is calculated as per the method described for connectivity-adjusted ecosystem condition (Equation 4 –Equation 9), substituting the ecosystem condition values for grid cells, nodes and edges (h_i, h_g, h_q) in the multi-resolution neighbourhood (Figure S1.2) with their "protected-connected" equivalents (ϕ_i, ϕ_g, ϕ_q).

The PARC-connectedness value for a grid cell is the relative amount of total protected-connected habitat to that cell, reported only for grid cells with $p_i > 0$:

$$PARCcon_i = \Gamma_{i,rel} \quad \text{Equation 23}$$

The PARC-connectedness value for any larger reporting region can be derived, and expressed, in two different ways. The first of these alternatives involves reporting the average of $PARCcon_i$ values across all protected cells within the region of interest. A property of this option, which some users may find disconcerting, is that the average connectivity of all protected cells within a region can decline over time if additions to the protected-area system are poorly connected to existing protected areas. The alternative approach, which we adopt here, involves summing the $PARCcon_i$ values of all protected cells and then dividing this sum by the total number of cells (both protected and unprotected) within the region of interest. The resulting value can then be interpreted as an estimate of the proportion of that region (e.g. a country) covered by protected areas (and OECMs) adjusted for the connectivity of these areas to one another, and to unprotected natural vegetation in the surrounding landscape. This connectivity-adjusted proportion will always be less than or equal to the raw (unadjusted) proportion of the region protected. A further, and arguably desirable, property of this approach is that the resulting proportion can only ever increase, not decrease, over time as additional areas are protected, provided that there is no coincidental decline in the condition of natural habitat in the surrounding landscape. To implement this approach, $PARCcon_r$ for a given region r containing R grid cells is calculated as:

$$PARCcon_r = \frac{\sum_{i=1}^{R} p_i PARCcon_i}{R} \qquad \text{Equation 24}$$

where the contribution of each protected cell is weighted by the proportion of land in that cell that is protected (p_i). If, for any reason, PARC-connectedness needs to be expressed in terms of the first of the above options – i.e. as an average of $PARCcon_i$ values across protected cells within that region – then this average can be derived simply by dividing any reported value of $PARCcon_r$ by the raw (unadjusted) proportion of the region covered by protected areas (or OECMs) for the relevant year.

As for the other indicators, for every country we also calculate PARC-connectedness values treating the country as a closed system ($PARCcon_c$) – hence, in all the above equations, comparing each focal cell i only with those other grid cells j falling within that country. This closed-system PARC-connectedness value is reported alongside the standard PARC- connectedness (i.e. open system) value for each country.

Table S5.4. Definition of mathematical terms used.

Term	Definition	Method section
α_l	proportion of species remaining under land use class l	Land use to condition
A_l	equivalent area of habitat remaining under land use class l	Land use to condition
A_{ref}	equivalent area of habitat remaining under reference condition	Land use to condition
b	An evenly spaced bin of compositional similarity values	BHI/PARC-rep
$BERI_i$	The BERI value for the focal cell i	BERI
$BERI_r$	The BERI value for any larger reporting region r	BERI
BHI_i	The BHI for grid cell i	BHI
BHI_r	The BHI value for any larger reporting region r	BHI
C_{ik}	The amount of accessible connected habitat in the landscape surrounding grid cell i which is projected to support a similar assemblage of species under climate scenario k	BERI
D_q	The condition-weighted length of each edge	Connected condition
d_{ig}	the condition weighted distance of the least cost path from focal cell i to node g	Connected condition
g	The focal node	Connected condition, BERI
h_q	average ecosystem condition at the head node of the edge q	Connected condition
h_i	the ecosystem condition value of cell i	Connected condition
$h_{i,con}$	the connectivity-adjusted ecosystem condition value for focal cell i	Connected condition
$h_{j,con}$	the connectivity-adjusted ecosystem condition value for cell j	BHI
h_j	the ecosystem condition value of node j	Connected condition
h_l	ecosystem condition for land use class l	Land use to condition
H_{ig}	The degree to which node g offers connected habitat to the focal cell i	Connected condition
i	focal grid cell	Connected condition
j	A grid cell	all
K_{ig}	the link permeability from focal cell i to node g	Connected condition
k	A climate scenario	BERI
l	Land use class	Land use to condition
L_q	length of edge q	Connected condition
λ	median dispersal distance (km)	Connected condition
m	The number of climate scenarios	BERI
M	the scalar for the degree to which low ecosystem condition increases the cost to movement	Connected condition
n	The number of grid cells	BHI
N	The number of nodes in the multi-resolution neighbourhood	Connected condition
n_{edge}	The number of intervening edges in the graph	Connected condition
p_i	The proportion of land covered by protected areas and OECMs in grid cell i	PARC
$PARCrep_i$	The PARC-representativeness value for each grid cell i	PARC-rep
$PARCrep_r$	The PARC-representativeness value for any larger reporting region r	PARC-rep
$PARCcon_i$	The PARC-connectedness value for each grid cell i	PARC-con
$PARCcon_r$	The PARC-connectedness value for any larger reporting region r	PARC-con
ϕ_i	The maximum of the ecosystem condition of cell i and the proportion of land protected in cell i	PARC-con
ϕ_g	The maximum of the ecosystem condition of node g and the proportion of land protected for node g	PARC-con
ϕ_q	The maximum of the ecosystem condition of edge q and the proportion of land protected for edge q	PARC-con
q	The focal edge	Connected condition
r	The number of bins the compositional similarity space is broken into	BHI, PARC-rep
R	The number of grid cells falling within a reporting region	All
ref	Reference condition	Land use to condition
s_{ij}	the predicted compositional similarity between the focal grid cell i and grid cell j	BHI
$s_{l,ref}$	Similarity of land use class l to reference	Land use to condition
t	The number of years from current to future climate	BERI
Γ_i	total connected habitat to focal cell i , from all k nodes in the multi-resolution neighbourhood	Connected condition
$\Gamma_{i,rel}$	relative amount of total connected habitat to focal cell i	Connected condition
$\Gamma_{i,max}$	the maximum possible total connected habitat	Connected condition
u	A constant used in the dispersal kernel (value = 5.8)	BERI
v	The number of median dispersal distances considered	BERI
w_i	The weight given to each cell i based (inversely) on its predicted compositional similarity to al other cells	BHI
z	species-area exponent	BHI, Land use to condition

References

Allnutt, T. F., S. Ferrier, G. Manion, G. V. N. Powell, T. H. Ricketts, B. L. Fisher, and F. Rakotondrainibe. 2008. "A Method for Quantifying Biodiversity Loss and Its Application to a 50-Year Record of Deforestation across Madagascar." *Conservation Letters* 1(4):173–81. doi:10.1111/j.1755-263X.2008.00027.x.

Brooks, Mollie, E., Kasper Kristensen, Koen Benthem J. ,van, Arni Magnusson, Casper Berg W., Anders Nielsen, Hans Skaug J., Martin Mächler, and Benjamin Bolker M. 2017. "glmmTMB Balances Speed and Flexibility Among Packages for Zero-Inflated Generalized Linear Mixed Modeling." *The R Journal* 9(2):378. doi:10.32614/RJ-2017-066.

Brus, D. J. 2019. "Sampling for Digital Soil Mapping: A Tutorial Supported by R Scripts." *Geoderma* 338:464–80. doi:10.1016/j.geoderma.2018.07.036.

CIESIN. 2018. "Gridded Population of the World, Version 4 (GPWv4): Population Count." *Revision* 11(Version 4.11).

Di Marco, M., S. Ferrier, T. D. Harwood, A. J. Hoskins, and J. E. M. Watson. 2019. "Wilderness areas halve the extinction risk of terrestrial biodiversity." *Nature* 573:582–85. doi:10.1038/s41586-019-1567-7.

Di Marco, M., T. D. Harwood, A. J. Hoskins, C. Ware, S. L. L. Hill, and S. Ferrier. 2019. "Projecting Impacts of Global Climate and Land-Use Scenarios on Plant Biodiversity Using Compositional-Turnover Modelling." *Global Change Biology* 25(8):2763–78. doi:10.1111/gcb.14663.

DiMiceli, C., R. Sohlberg, and J. Townshend. 2022. "MODIS/Terra Vegetation Continuous Fields Yearly L3 Global 250m SIN Grid V061 [Data Set."

Drielsma, Michael, Simon Ferrier, Gary Howling, Glenn Manion, Subhashni Taylor, and Jamie Love. 2014. "The Biodiversity Forecasting Toolkit: Answering the 'How Much', 'What', and 'Where' of Planning for Biodiversity Persistence." *Ecological Modelling* 274:80–91. doi:10.1016/j.ecolmodel.2013.11.028.

Drielsma, Michael, Simon Ferrier, and Glenn Manion. 2007. "A Raster-Based Technique for Analysing Habitat Configuration: The Cost–Benefit Approach." *Ecological Modelling* 202(3–4):324–32. doi:10.1016/j.ecolmodel.2006.10.016.

ESA. 2017. *ESA Land Cover CCI Product User Guide Version 2*. *Technical Report*. maps.elie.ucl.ac.be/CCI/viewer/download/ESACCI-LC-Ph2-PUGv2_2.0.pdf.

Ferrier, S., T. D. Harwood, C. Ware, and A. J. Hoskins. 2020. "A Globally Applicable Indicator of the Capacity of Terrestrial Ecosystems to Retain Biological Diversity under Climate Change: The Bioclimatic Ecosystem Resilience Index." *Ecological Indicators* 117:106554. doi:10.1016/j.ecolind.2020.106554.

Ferrier, S., C. Ware, J. M. Austin, H. S. Grantham, T. D. Harwood, and J. E. M. Watson. 2024. "Ecosystem Extent Is a Necessary but Not Sufficient Indicator of the State of Global Forest Biodiversity." *Conservation Letters* 17(5):13045. doi:10.1111/conl.13045.

GADM. 2024. "Database of Global Administrative Areas."

García Martín, H., and N. Goldenfeld. 2006. "On the Origin and Robustness of Power-Law Species–Area Relationships in Ecology." *Proceedings of the National Academy of Sciences* 103(27):10310–15. doi:10.1073/pnas.0510605103.

Harwood, T., J. Love, M. Drielsma, C. Brandon, and S. Ferrier. 2022. "Staying Connected: Assessing the Capacity of Landscapes to Retain Biodiversity in a Changing Climate." *Landscape Ecology* 37(12):3123–39. doi:10.1007/s10980-022-01534-5.

Hijmans, Robert J., Susan E. Cameron, Juan L. Parra, Peter G. Jones, and Andy Jarvis. 2005. “Very High Resolution Interpolated Climate Surfaces for Global Land Areas.” *International Journal of Climatology* 25(15):1965–78. doi:10.1002/joc.1276.

Hoskins, A. J., A. Bush, J. Gilmore, T. Harwood, L. N. Hudson, C. Ware, and S. Ferrier. 2016. “Downscaling Land-Use Data to Provide Global 30'' Estimates of Five Land-Use Classes.” *Ecology and Evolution* 6(9):3040–55. doi:10.1002/ece3.2104.

Hoskins, A. J., T. D. Harwood, C. Ware, K. J. Williams, J. J. Perry, N. Ota, and S. Ferrier. 2020. “BILBI: Supporting Global Biodiversity Assessment through High-Resolution Macroecological Modelling.” *Environmental Modelling & Software* 132:104806. doi:10.1016/j.envsoft.2020.104806.

Hudson, L. N., T. Newbold, S. Contu, S. L. L. Hill, I. Lysenko, A. Palma, and A. Purvis. 2017. “The Database of the PREDICTS (Projecting Responses of Ecological Diversity In Changing Terrestrial Systems) Project.” *Ecology and Evolution* 7(1):145–88. doi:10.1002/ece3.2579.

Hudson, Lawrence N., Tim Newbold, Sara Contu, Samantha L. L. Hill, Igor Lysenko, Adriana De Palma, Helen R. P. Phillips, Rebecca A. Senior, Dominic J. Bennett, Hollie Booth, Argyrios Choimes, David L. P. Correia, Julie Day, Susy Echeverría-Londoño, Morgan Garon, Michelle L. K. Harrison, Daniel J. Ingram, Martin Jung, Victoria Kemp, Lucinda Kirkpatrick, Callum D. Martin, Yuan Pan, Hannah J. White, Job Aben, Stefan Abrahamczyk, Gilbert B. Adum, Virginia Aguilar-Barquero, Marcelo A. Aizen, Marc Ancrenaz, Enrique Arbeláez-Cortés, Inge Armbrecht, Badrul Azhar, Adrián B. Azpiroz, Lander Baeten, András Báldi, John E. Banks, Jos Barlow, Péter Batáry, Adam J. Bates, Erin M. Bayne, Pedro Beja, Åke Berg, Nicholas J. Berry, Jake E. Bicknell, Jochen H. Bihn, Katrin Böhning-Gaese, Teun Boekhout, Céline Boutin, Jérémy Bouyer, Francis Q. Brearley, Isabel Brito, Jörg Brunet, Grzegorz Buczkowski, Erika Buscardo, Jimmy Cabra-García, María Calviño-Cancela, Sydney A. Cameron, Eliana M. Cancello, Tiago F. Carrijo, Anelena L. Carvalho, Helena Castro, Alejandro A. Castro-Luna, Rolando Cerda, Alexis Cerezo, Matthieu Chauvat, Frank M. Clarke, Daniel F. R. Cleary, Stuart P. Connop, Biagio D’Aniello, Pedro Giovâni Da Silva, Ben Darvill, Jens Dauber, Alain Dejean, Tim Diekötter, Yamileth Dominguez-Haydar, Carsten F. Dormann, Bertrand Dumont, Simon G. Dures, Mats Dynesius, Lars Edenius, Zoltán Elek, Martin H. Entling, Nina Farwig, Tom M. Fayle, Antonio Felicioli, Annika M. Felton, Gentile F. Ficetola, Bruno K. C. Filgueiras, Steven J. Fonte, Lauchlan H. Fraser, Daisuke Fukuda, Dario Furlani, Jörg U. Ganzhorn, Jenni G. Garden, Carla Gheler-Costa, Paolo Giordani, Simonetta Giordano, Marco S. Gottschalk, Dave Goulson, Aaron D. Gove, James Grogan, Mick E. Hanley, Thor Hanson, Nor R. Hashim, Joseph E. Hawes, Christian Hébert, Alvin J. Helden, John-André Henden, Lionel Hernández, Felix Herzog, Diego Higuera-Diaz, Branko Hilje, Finbarr G. Horgan, Roland Horváth, Kristoffer Hylander, Paola Isaacs-Cubides, Masahiro Ishitani, Carmen T. Jacobs, Víctor J. Jaramillo, Birgit Jauker, Mats Jonsell, Thomas S. Jung, Vena Kapoor, Vassiliki Kati, Eric Katovai, Michael Kessler, Eva Knop, Annette Kolb, Ádám Kőrösi, Thibault Lachat, Victoria Lantschner, Violette Le Féon, Gretchen LeBuhn, Jean-Philippe Légaré, Susan G. Letcher, Nick A. Littlewood, Carlos A. López-Quintero, Mounir Louhaichi, Gabor L. Lövei, Manuel Esteban Lucas-Borja, Victor H. Luja, Kaoru Maeto, Tibor Magura, Neil Aldrin Mallari, Erika Marin-Spiotta, E. J. P. Marshall, Eliana Martínez, Margaret M. Mayfield, Grzegorz Mikusinski, Jeffrey C. Milder, James R. Miller, Carolina L. Morales, Mary N. Muchane, Muchai Muchane, Robin Naidoo, Akihiro Nakamura, Shoji Naoe, Guiomar Nates-Parra, Dario A. Navarrete Gutierrez, Eike L. Neuschulz, Norbertas Noreika, Olivia Norfolk, Jorge Ari Noriega, Nicole M. Nöske, Niall O’Dea, William Oduro, Caleb Ofori-Boateng, Chris O. Oke, Lynne M. Osgathorpe, Juan Paritsis, Alejandro Parra-H, Nicolás Pelegrin, Carlos A. Peres, Anna S. Persson, Theodora Petanidou, Ben Phalan, T. Keith Philips, Katja Poveda, Eileen F. Power, Steven J. Presley, Vânia Proença, Marino Quaranta, Carolina Quintero, Nicola A. Redpath-Downing, J. Leighton Reid, Yana T. Reis, Danilo B. Ribeiro, Barbara A. Richardson, Michael J. Richardson, Carolina A. Robles, Jörg Römbke, Luz Piedad Romero-Duque, Loreta Rosselli, Stephen J. Rossiter, T’ai H. Roulston, Laurent Rousseau, Jonathan P. Sadler, Szabolcs Sáfián, Romeo A. Saldaña-Vázquez, Ulrika Samnegård, Christof Schüepp, Oliver Schweiger, Jodi L. Sedlock, Ghazala Shahabuddin, Douglas Sheil, Fernando A. B. Silva, Eleanor M. Slade, Allan H. Smith-Pardo, Navjot S. Sodhi, Eduardo J. Somarriba, Ramón A. Sosa, Jane

C. Stout, Matthew J. Struebig, Yik-Hei Sung, Caragh G. Threlfall, Rebecca Tonietto, Béla Tóthmérész, Teja Tscharntke, Edgar C. Turner, Jason M. Tylianakis, Adam J. Vanbergen, Kiril Vassilev, Hans A. F. Verboven, Carlos H. Vergara, Pablo M. Vergara, Jort Verhulst, Tony R. Walker, Yanping Wang, James I. Watling, Konstans Wells, Christopher D. Williams, Michael R. Willig, John C. Z. Woinarski, Jan H. D. Wolf, Ben A. Woodcock, Douglas W. Yu, Andrey S. Zaitsev, Ben Collen, Rob M. Ewers, Georgina M. Mace, Drew W. Purves, Jörn P. W. Scharlemann, and Andy Purvis. 2014. "The PREDICTS Database: A Global Database of How Local Terrestrial Biodiversity Responds to Human Impacts." *Ecology and Evolution* 4(24):4701–35. doi:10.1002/ece3.1303.

Hurtt, George C., Louise Chini, Ritvik Sahajpal, Steve Frolking, Benjamin L. Bodirsky, Katherine Calvin, Jonathan C. Doelman, Justin Fisk, Shinichiro Fujimori, Kees Klein Goldewijk, Tomoko Hasegawa, Peter Havlik, Andreas Heinimann, Florian Humpenöder, Johan Jungclaus, Jed O. Kaplan, Jennifer Kennedy, Tamás Krisztin, David Lawrence, Peter Lawrence, Lei Ma, Ole Mertz, Julia Pongratz, Alexander Popp, Benjamin Poulter, Keywan Riahi, Elena Shevliakova, Elke Stehfest, Peter Thornton, Francesco N. Tubiello, Detlef P. Van Vuuren, and Xin Zhang. 2020. "Harmonization of Global Land Use Change and Management for the Period 850–2100 (LUH2) for CMIP6." *Geoscientific Model Development* 13(11):5425–64. doi:10.5194/gmd-13-5425-2020.

Ikotun, A. M., A. E. Ezugwu, L. Abualigah, B. Abuhaija, and J. Heming. 2023. "K-Means Clustering Algorithms: A Comprehensive Review, Variants Analysis, and Advances in the Era of Big Data." *Information Sciences* 622:178–210. doi:10.1016/j.ins.2022.11.139.

Marco, M., T. D. Harwood, A. J. Hoskins, C. Ware, S. L. L. Hill, and S. Ferrier. 2019. "Projecting Impacts of Global Climate and Land-Use Scenarios on Plant Biodiversity Using Compositional-Turnover Modelling." *Global Change Biology* 25(8):2763–78. doi:10.1111/gcb.14663.

McInerney, D., R. Lempert, and K. Keller. 2012. "What Are Robust Strategies in the Face of Uncertain Climate Threshold Responses?" *Climatic Change* 112(3):547–68. doi:10.1007/s10584-011-0377-1.

Mokany, Karel, Simon Ferrier, Thomas D. Harwood, Chris Ware, Moreno Di Marco, Hedley S. Grantham, Oscar Venter, Andrew J. Hoskins, and James E. M. Watson. 2020. "Reconciling Global Priorities for Conserving Biodiversity Habitat." *Proceedings of the National Academy of Sciences* 117(18):9906–11. doi:10.1073/pnas.1918373117.

Newbold, T., L. N. Hudson, S. L. L. Hill, S. Contu, C. L. Gray, J. P. W. Scharlemann, and A. Purvis. 2016. "Global Patterns of Terrestrial Assemblage Turnover within and among Land Uses." *Ecography* 39(12):1151–63. doi:10.1111/ecog.01932.

Olson, D. M., E. Dinerstein, E. D. Wikramanayake, N. D. Burgess, G. V. N. Powell, E. C. Underwood, and K. R. Kassem. 2001. "Terrestrial Ecoregions of the World: A New Map of Life on Earth: A New Global Map of Terrestrial Ecoregions Provides an Innovative Tool for Conserving Biodiversity." *Bioscience* 51(11):933–38. doi:10.1641/0006-3568(2001)051.

Pedregosa, F., G. Varoquaux, A. Gramfort, V. Michel, B. Thirion, O. Grisel, and E. Duchesnay. 2011. "Scikit-Learn: Machine Learning in Python." *Journal of Machine Learning Research* 12:2025–2830.

Rosenzweig, M. L. 1995. *Species Diversity in Space and Time*. Cambridge: Cambridge University Press.

United Nations. 2024. "System of Environmental-Economic Accounting—Ecosystem Accounting (SEEA EA). Statistical Papers." *Series F* (124). https://seea.un.org/ecosystem-accounting.

Appendix S2: Metadata

Table S2.1. Output and summary metadata. Indicator is one of: BHI, BERI, PARC-rep, or PARC-conn. Year is a year within the current timeseries (2000-2024)

Dataset	Naming	Notes
Annual global indicator GeoTIFF files (2000 – 2024)	{indicator}-{year}.tif	Single file per year of grid cell level indicator values.
Annual country summaries	{indicator}-countries.csv	Indicator summarised using GADM country borders.
Annual country summaries (bordered)	{indicator}-countries-bordered.csv	Indicator run with closed border approach using GADM country borders.
Annual biome summaries with countries	{indicator}-{country}-biome.csv	Indicator summarised using WWF biome boundaries within individual GADM country borders.